



This is a repository copy of *Energy efficiency maximization for UAV-enabled hybrid backscatter-harvest-then-transmit communications*.

White Rose Research Online URL for this paper:

<https://eprints.whiterose.ac.uk/221953/>

Version: Accepted Version

Article:

Yang, H. orcid.org/0000-0002-7675-1543, Ye, Y. orcid.org/0000-0002-0110-3592, Chu, X. orcid.org/0000-0003-1863-6149 et al. (1 more author) (2022) Energy efficiency maximization for UAV-enabled hybrid backscatter-harvest-then-transmit communications. *IEEE Transactions on Wireless Communications*, 21 (5). pp. 2876-2891. ISSN 1536-1276

<https://doi.org/10.1109/twc.2021.3116509>

© 2021 IEEE. Personal use of this material is permitted. Permission from IEEE must be obtained for all other users, including reprinting/ republishing this material for advertising or promotional purposes, creating new collective works for resale or redistribution to servers or lists, or reuse of any copyrighted components of this work in other works. Reproduced in accordance with the publisher's self-archiving policy.

Reuse

Items deposited in White Rose Research Online are protected by copyright, with all rights reserved unless indicated otherwise. They may be downloaded and/or printed for private study, or other acts as permitted by national copyright laws. The publisher or other rights holders may allow further reproduction and re-use of the full text version. This is indicated by the licence information on the White Rose Research Online record for the item.

Takedown

If you consider content in White Rose Research Online to be in breach of UK law, please notify us by emailing eprints@whiterose.ac.uk including the URL of the record and the reason for the withdrawal request.



eprints@whiterose.ac.uk
<https://eprints.whiterose.ac.uk/>

Energy Efficiency Maximization for UAV-Enabled Hybrid Backscatter-Harvest-then-Transmit Communications

Haohang Yang, Yinghui Ye, Xiaoli Chu, *Senior Member, IEEE*, Sumei Sun, *Fellow, IEEE*

Abstract

Wireless powered communication via backscatter and/or harvest-then-transmit (HTT) has been considered a promising solution to connecting nodes in the Internet of things (IoT) networks. However, the harvested energy at an IoT node is heavily limited by the distance between the node and the power beacon (PB) due to the high propagation loss. In this paper, we propose to employ an unmanned aerial vehicle (UAV) as a mobile PB to provide energy signals on demand to the IoT nodes, which convey their information to a reader via backscattering or active transmission using the harvested energy. We maximize the total energy efficiency (EE) of all the IoT nodes powered by the UAV by jointly optimizing the UAV's transmit power and trajectory, the IoT nodes' backscatter reflection coefficients and their transmit power for active transmission, and the time allocation between backscattering and active transmission. To solve the formulated non-linear fractional programming problem, we use the generalized fractional programming theory and a block coordinated decent method to decompose it into two sub-problems: one optimizes the communication resource allocation under a fixed UAV trajectory, and the other optimizes the UAV trajectory with given communication resource allocation. We then devise a Dinkelbach-based iterative algorithm to solve the two sub-problems by employing a Lagrangian dual method and a successive convex programming technique, respectively and iteratively. Simulation results show that our proposed iterative algorithm converges very fast, and the optimized UAV-enabled hybrid backscatter-HTT communication achieves a much higher EE of all the IoT nodes than the benchmark schemes including the UAV-enabled backscatter, UAV-enabled HTT, and hybrid BackCom-HTT with a fixed PB.

Index Terms

Backscatter communication, energy efficiency, harvest then transmit, resource allocation, unmanned aerial vehicle, trajectory, wireless power transfer.

Haohang Yang and Xiaoli Chu are with the Department of Electronic and Electrical Engineering, University of Sheffield, Sheffield, S1 4ET, United Kingdom (e-mail: hyang42@sheffield.ac.uk, x.chu@sheffield.ac.uk).

Yinghui Ye is with the Shaanxi Key Laboratory of Information Communication Network and Security, Xi'an University of Posts & Telecommunications, China (e-mail: connectyyh@126.com).

S. Sun is with the Institute for Infocom Research, A*STAR, 138632, Singapore (e-mail: sunsm@i2r.a-star.edu.sg).

I. INTRODUCTION

DUE to the limited battery capacity of low-powered Internet of Things (IoT) nodes, wireless powered communication networks (WPCNs) have been proposed to support IoT, where the IoT nodes can either harvest RF energy from an energy source and then use the harvested energy to convey information via active transmission, i.e., harvest-then-transmit (HTT) [1]–[4], or modulate and backscatter the incident radio frequency (RF) signal to carry its information to the associated receiver without requiring an active transceiver [5]–[8]. The circuit power consumption of backscatter communications (BackCom) is very low and can be supported by the harvested RF energy. However, BackCom cannot realize when the incident signals are not available. Meanwhile, HTT can solve this problem but its energy consumption is normally high [5]–[8]. To exploit the complementarity of BackCom and HTT, hybrid BackCom-HTT communications have been proposed. The authors in [8] solved a max-min throughput problem among multiple sensor nodes for a wireless powered IoT network. In [9], the wireless powered nodes were allowed to operate in backscatter mode when the harvested energy from the dedicated RF signals is not sufficient to support HTT, where the time allocated for backscattering was optimized to maximize the throughput. The authors in [10] proposed hybrid BackCom-HTT for a cognitive WPCN, where the throughput of the secondary communication system was maximized by optimizing the time allocation between backscattering and energy harvesting and that between the bistatic backscatter mode and the HTT mode. In [11], the time allocation between data backscattering and energy harvesting, as well as the time sharing among multiple transmitters were optimized to maximize the throughput of a RF-powered backscatter cognitive radio network. The authors in [12] maximized the energy efficiency (EE) of all the devices in a hybrid BackCom-HTT network by optimizing the transmit power of the power beacon (PB) and hybrid devices, and the time allocation among energy harvesting, the backscatter mode and the HTT mode.

Although the above works [9]–[12] demonstrated the superior performance of hybrid BackCom-HTT over BackCom or HTT in terms of throughput and EE, they considered a fixed RF energy source, e.g., a PB, where the received power at IoT nodes is limited by their distance to the PB due to severe RF propagation loss [13]. Recently, unmanned aerial vehicles (UAVs) have been employed as mobile PB to provide RF energy to IoT nodes via line-of-sight (LoS) links. In [14], the UAV's trajectory was optimized to maximize the total energy harvested by all the IoT nodes wirelessly powered by it. In [15], a max-min throughput problem was solved in a UAV-enabled WPCN, where a UAV was dispatched as a mobile access point (AP). In [16], the system throughput of a UAV-aided BackCom network was maximized by optimizing the time allocation, backscatter reflection coefficient, and UAV trajectory for two protocols, namely transmit-backscatter and transmit-backscatter-relay, where the direct link from the backscatter device to the receiver of the latter protocol is not available. In [17], two UAVs were used to wirelessly power two IoT devices and collect information from them, and the minimum uplink throughput of the two IoT devices was maximized through jointly optimizing the trajectories of the two UAVs and the downlink/uplink wireless resource allocation. The above works indicate that the UAV-enabled networks can achieve better performance in terms of

throughput and energy transmission compared with fixed PB based networks. However, we note that UAV-carried mobile PB has not been exploited for emerging hybrid BackCom-HTT networks. This motivates us to configure a new network which fully makes the use of the advantages of UAV and BackCom-HTT.

In this paper, we propose a novel UAV-enabled hybrid BackCom-HTT communication system to connect multiple IoT nodes to a reader, where a UAV is dispatched as a mobile PB to provide RF energy for all the IoT nodes. Based on a time-division multiple access (TDMA) protocol, an IoT node first backscatters the incident RF signal from the UAV to carry its own information to the reader, while harvesting the RF power for supporting its circuit operation together with the other IoT nodes, and then utilizes the remaining energy to transmit information to the reader via active transmission. We then maximize the total EE of all the IoT nodes wirelessly powered by the UAV.

Our main contributions are summarized as follows:

- We propose a novel system model, namely the UAV-enabled hybrid BackCom-HTT communication network, where a UAV works as a mobile energy source to provide RF energy for all the ground IoT nodes. The IoT nodes utilize the incident RF signal to communicate with a reader via a hybrid BackCom-HTT scheme.
- To exploit the synergy between hybrid BackCom-HTT communications and UAV, we formulate a problem to maximize the EE of all the IoT nodes in the UAV-enabled hybrid BackCom-HTT system by jointly optimizing the UAV's transmit power and trajectory and the allocation of communication resources, including the backscatter reflection coefficients, the transmit power of IoT nodes during active transmission, and the time allocation between BackCom and active transmission.
- Since the EE of multiple IoT nodes are jointly maximized, the formulated optimization problem involves many variables that are coupled in the objective function and/or the constraints. Through theoretical analysis, we reveal that letting the UAV transmit with the maximum power maximizes the EE of all the IoT nodes. Leveraging this finding and the generalized fractional programming theory, we transform the original optimization problem into a more tractable but still non-convex problem. Then, we use a block coordinated decent (BCD) method to decompose the transformed problem into two sub-problems: one optimizes the communication resource allocation with a fixed UAV trajectory and the other optimizes the UAV trajectory with given communication resource allocation. We employ a Lagrangian dual method to solve the former sub-problem optimally and apply a successive convex programming (SCP) technique to obtain a locally optimal solution to the latter sub-problem. The closed-form expressions for the optimal reflection coefficient and active transmit power of each IoT node are derived. Based on the obtained solutions, we propose a Dinkelbach based iterative algorithm to maximize the EE of all the IoT nodes in the UAV-enabled hybrid BackCom-HTT system.
- We perform extensive simulations to evaluate the optimized UAV trajectory, time allocation for BackCom and active transmission, the convergence of our proposed iterative algorithm, and the EE of all the IoT nodes achieved by our proposed algorithm in comparison with that of several benchmark schemes including the UAV-enabled backscatter, UAV-enabled HTT, energy consumption minimization, and hybrid BackCom-HTT with a fixed PB. The simulation results show that the proposed algorithm has a fast convergence speed, and

can achieve a much higher total EE than the benchmark schemes. In addition, we observe that a higher EE is achieved for all the IoT nodes when more time is allocated to those IoT nodes with better channel conditions to the UAV and the reader for BackCom and active transmissions, respectively. Also, the UAV tends to fly towards to those IoT nodes with better channel condition.

The rest of the paper is organized as follows. The system model of a UAV-enabled hybrid BackCom-HTT network is built in Section II. In Section III, the total EE maximization problem is formulated and solved. Section IV analyzes the convergence and computational complexity of our proposed algorithms. In Section V, the numerical results are presented. Section VI concludes the paper.

II. SYSTEM MODEL

In this section, we present the system model, and the associated throughput analysis and definition of the total EE.

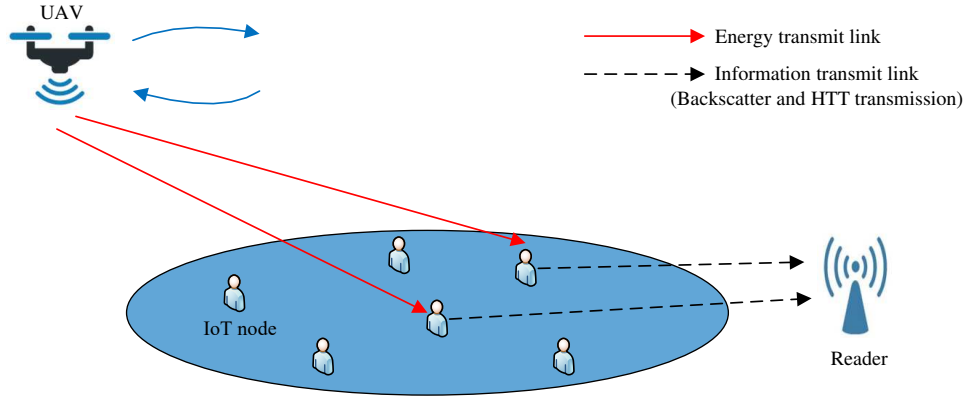


Fig. 1: UAV-enabled hybrid BackCom-HTT network.

A. Network Model

As illustrated in Fig. 1, the proposed UAV-enabled hybrid BackCom-HTT network consists of one UAV, M IoT nodes and one reader, where the IoT nodes harvest energy from the UAV's RF transmission and transmit information to the reader through hybrid BackCom and HTT within the time block T . We assume that each IoT node is equipped with a backscatter circuit, an EH module, and an active RF transmitter such that they can operate in the BackCom and HTT modes. Each IoT node $i \in \mathcal{M} = \{1, \dots, M\}$ is deployed at a fixed location $q_i^g = (x_i, y_i)$ on the ground in a 2-D Cartesian coordinate system. The reader is fixed at the location $q^r = (x^r, y^r)$. The UAV is assumed to fly at a fixed altitude $H > 0$ above the ground, and the location of the UAV in the 2D horizontal plane at altitude H at any time instant $t \in T$ is denoted by $q_t^u = (x_t^u, y_t^u)$. We assume that all the IoT nodes are inside a region on the ground, while the UAV is dispatched from an initial location $q_{ini}^u = (x_{ini}^u, y_{ini}^u)$ outside this region to provide energy for the IoT nodes and then flies back to q_{ini}^u at the end of the BackCom time period.

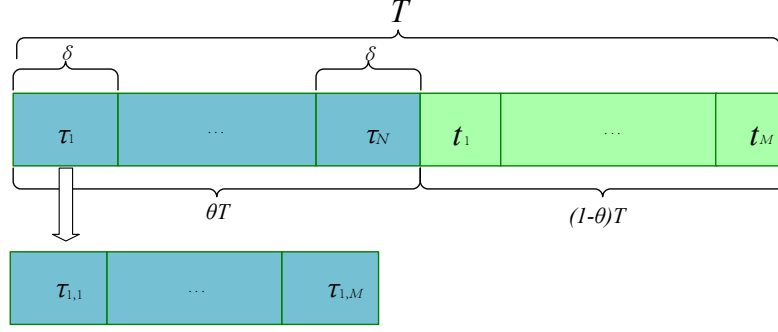


Fig. 2: Time allocation scheme.

The entire time block T is divided into two time periods, i.e., θT ($0 < \theta \leq 1$) for BackCom and $(1 - \theta)T$ for HTT active transmission by utilizing the energy harvested within θT , as shown in Fig. 2. During the first time period, a UAV is dispatched to provide energy for the IoT nodes to backscatter their own information to the reader via BackCom, and the IoT node-to-reader BackComs follow a TDMA protocol. For simplicity, the first time period of θT is equally divided into N time slots, where the n -th time slot $\tau_n, n \in \mathcal{N} = \{1, 2, \dots, N\}$, has a duration of $\delta = \frac{\theta T}{N}$. We assume that the value of N is sufficiently large so that the UAV can be considered as static at each time slot [14]–[16], and $N \gg M$. Let q_n^u denote the location of the UAV at time slot n . Thus, the distance between the UAV and IoT node i at time slot n is given by

$$d_{i,n}^u = \sqrt{\|q_n^u - q_i^g\|^2 + H^2}, \quad (1)$$

where $\|\cdot\|$ denotes the Euclidean norm of a vector.

Following [16], [18], [19], we adopt the following Rician fading channel model for UAV communications:

$$h_{i,n}^u = \beta_0 (d_{i,n}^u)^{-2} \|\mu_{i,n}^{(1)}\|^2 = \frac{\beta_0 \|\mu_{i,n}^{(1)}\|^2}{\|q_n^u - q_i^g\|^2 + H^2}, \quad (2)$$

where β_0 denotes the channel power gain at a reference distance of $d_0 = 1\text{m}$, and $\mu_{i,n}^{(1)}$ denotes the small-scale fading and is modeled as

$$\mu_{i,n}^{(1)} = \sqrt{\frac{K}{K+1}} \mu_{i,n}^{\hat{(1)}} + \sqrt{\frac{1}{K+1}} \mu_{i,n}^{\hat{(1)}}, \quad (3)$$

where $\mu_{i,n}^{\hat{(1)}}$ denotes the LoS channel coefficient with $\|\mu_{i,n}^{\hat{(1)}}\| = 1$, $\mu_{i,n}^{\hat{(1)}}$ represents the non-LoS channel coefficient, which is a circularly symmetric complex Gaussian random variable with mean zero and variance 1, and K is the Rician factor. In this paper, it is reasonable to assume that the channel from the UAV to an IoT node is dominated by the LoS path [20]–[23]. Thus, the Rician factor K is very large, and the channel model in (2) approximately reduces to $h_{i,n}^u = \beta_0 (d_{i,n}^u)^{-2} \|\mu_{i,n}^{\hat{(1)}}\|^2$, which is equivalent to a free-space path-loss model [16]. Hence, the channel from the UAV to an IoT node can be estimated based on the locations of the UAV and IoT nodes.

To ensure that every IoT node has a chance to backscatter its information to the reader in each time slot, a time slot is further divided into M sub-slots [15], where the i th sub-slot is allocated to IoT node i . Let $\tau_{i,n}$ denote the backscattering time for IoT node i at time slot n and $\sum_{i=1}^M \tau_{i,n} = \frac{\theta T}{N}$ holds for $\forall n \in \mathcal{N}$.

When IoT node i is in the backscatter mode, its received RF signal from the UAV is divided into two parts [7]: a $Z_{i,n}$ portion of the received power is used for BackCom to the reader, and the rest is harvested for supporting its circuit consumption, where $Z_{i,n} \in [0, 1]$ is the reflection coefficient¹. Accordingly, the total amount of energy harvested by IoT node i during the first time period θT is given by

$$EH_i = \sum_{n=1}^N \left(P^u \eta h_{i,n}^u (1 - Z_{i,n}) \tau_{i,n} + P^u \eta h_{i,n}^u \left(\frac{\theta T}{N} - \tau_{i,n} \right) \right) = \sum_{n=1}^N P^u \eta h_{i,n}^u \left(\frac{\theta T}{N} - \tau_{i,n} Z_{i,n} \right). \quad (4)$$

where P^u represents the UAV transmit power, η is the energy conversion efficiency of the EH circuit, which is assumed to include the EH circuit power consumption. We ignore the energy harvested from the signals backscattered by the other IoT nodes and the thermal noise, since their power is much smaller than P^u [9], [10], [12].

During the second time period of $(1 - \theta)T$, the IoT nodes utilize the remaining harvested energy (after deducting the circuit energy consumption) to transmit information to the reader via active transmission. Same as in BackCom period, TDMA is used. We divide $(1 - \theta)T$ into M time slots, where the i th time slot of duration t_i is allocated to the i th IoT node for active transmission, and we have $\sum_{i=1}^M t_i = (1 - \theta)T$.

B. Throughput of BackCom and HTT

The sum received power at the reader from IoT node i via BackCom and from the UAV at time slot n is given by [25]

$$P_{i,n}^{r,B} = P^u Z_{i,n} h_{i,n}^u h_i^r + P^u h_n^{u,r}, \quad (5)$$

where $h_i^r = \beta_0 (d_i^r)^{-\alpha} \|\mu_i^{(2)}\|^2$ denotes the channel power gain from IoT node i to the reader and $d_i^r = \|q_i^g - q^r\|$, where α is the free space path loss exponent and $\|\mu_i^{(2)}\|^2$ represents the Rayleigh fading power gain. The channel power gain from the UAV to the reader is denoted as $h_n^{u,r}$. Since the UAV serves as the dedicated energy source, its transmitted signal is a priori known to the reader, and the interference $P^u h_n^{u,r}$ can be removed by the reader. After the UAV interference has been removed, the received power at the reader at time slot n is rewritten as $P_{i,n}^{r,B'} = P^u Z_{i,n} h_{i,n}^u h_i^r$ [26].

Thus, the BackCom throughput of IoT node i -to-reader link at time slot n can be calculated as

$$R_{i,n}^B = W \tau_{i,n} \log_2 \left(1 + \frac{\varphi P_{i,n}^{r,B'}}{W \sigma^2} \right), \quad (6)$$

¹The backscattered signal is composed of two components: the structural mode scattering component and the antenna mode scattering component. In this paper, we only consider the antenna mode scattering component, which is characterized by the reflection coefficient, because the structural mode scattering is determined by the geometrical layout of the reflective device antenna and the electromagnetic properties of the material, and can be regarded as a constant value [24].

where W is the system bandwidth. Since BackCom usually transmits modulated signals from a finite constellation, which is very different from Gaussian signaling widely adopted in conventional active communications, thus the conventional achievable rate formula cannot perfectly match with that in BackCom. We introduce φ to represent the performance gap between the active transmission and the BackCom [8]–[12], and σ^2 denotes the noise power spectral density.

The received power at the reader from the active transmission of IoT node i is given by

$$P_i^{r,H} = P_i h_i^r, \quad (7)$$

where P_i denotes the transmit power of IoT node i .

Then, the active transmission throughput of IoT node i -to-reader link is calculated as

$$R_i^H = W t_i \log_2 \left(1 + \frac{P_i^{r,H}}{W \sigma^2} \right). \quad (8)$$

C. Total Energy Efficiency

The total EE of all the IoT nodes is defined as the ratio of the total throughput achieved by the IoT nodes to the total energy consumption of the IoT nodes [27]². Letting R_{sum} denote the total throughput achieved by all the IoT nodes in T , we have

$$R_{sum} = \sum_{i=1}^M \sum_{n=1}^N R_{i,n}^B + \sum_{i=1}^M R_i^H. \quad (9)$$

The energy consumption of IoT node i is given by $EC_i = \sum_{n=1}^N P_{cir}^B \tau_{i,n} + (P_{cir}^H + P_i) t_i$, where P_{cir}^B and P_{cir}^H represent the constant circuit power consumption for BackCom and active transmission, respectively, and they are assumed to be the same for all M IoT nodes.

The total energy consumption of all the IoT nodes is given by

$$EC_{sum} = \sum_{i=1}^M \sum_{n=1}^N P_{cir}^B \tau_{i,n} + \sum_{i=1}^M (P_{cir}^H + P_i) t_i, \quad (10)$$

Then, the total EE of all the IoT nodes is given by

$$EE_{sum} = \frac{R_{sum}}{EC_{sum}}. \quad (11)$$

III. ENERGY EFFICIENCY MAXIMIZATION

In this section, we first formulate the EE maximization problem for the considered UAV-aided hybrid BackCom-HTT IoT system, then we propose a Dinkelbach-based iterative algorithm to solve the optimization problem.

²In this paper, we aim to maximize the total EE of all the IoT nodes by jointly optimizing how they harvest and use the RF energy transmitted by the UAV, which can be regarded as maximizing the efficiency of the IoT nodes in utilizing the RF energy provided by the UAV [12], [27]. The system EE that includes the UAV's energy consumption will be studied in our future work.

A. Problem Formulation

We propose to maximize the EE of all the IoT nodes by jointly optimizing the UAV's transmit power P^u , transmit time factor θ , and trajectory vector $\mathbf{q} = [q_1^u, q_2^u, \dots, q_N^u]$, as well as the IoT nodes' BackCom reflection coefficient vectors $\mathbf{Z}_n = [Z_{1,n}, Z_{2,n}, \dots, Z_{M,n}]$, $n \in \mathcal{N}$, BackCom time allocation vectors $\boldsymbol{\tau}_n = [\tau_{1,n}, \tau_{2,n}, \dots, \tau_{M,n}]$, $n \in \mathcal{N}$, active transmission time allocation vector $\mathbf{t} = [t_1, t_2, \dots, t_M]$, and active transmission power vector $\mathbf{P} = [P_1, P_2, \dots, P_M]$. Accordingly, the optimization problem is formulated as

$$\begin{aligned}
 \mathbf{P}_1 : \quad & \max_{\{P^u, \theta, \mathbf{Z}_n, \boldsymbol{\tau}_n, \mathbf{t}, \mathbf{P}, \mathbf{q}\}} EE_{sum} \\
 \text{s.t.} \quad & \\
 \text{C1 : } & 0 \leq \theta \leq 1, 0 \leq Z_{i,n} \leq 1, \tau_{i,n} \geq 0, t_i \geq 0, \forall i, \forall n; \\
 \text{C2 : } & 0 \leq P^u \leq P_{\max}^{\text{UAV}}, 0 \leq P_i \leq P_{\max}^{\text{node}}, \forall i; \\
 \text{C3 : } & \sum_{i=1}^M \tau_{i,n} = \frac{\theta T}{N}; \sum_{i=1}^M t_i = (1 - \theta)T, \forall n; \\
 \text{C4 : } & \sum_{n=1}^N R_{i,n}^B + R_i^H \geq R_{\min}, \forall i; \\
 \text{C5 : } & 0 \leq P_i t_i \leq EH_i - \sum_{n=1}^N P_{\text{cir}}^B \tau_{i,n} - P_{\text{cir}}^H t_i, \forall i; \\
 \text{C6 : } & EH_i - EC_i \geq 0, \forall i; \\
 \text{C7 : } & \|q_n^u - q_{n-1}^u\| \leq V_{\max} \delta, \forall n; \\
 \text{C8 : } & q_1^u = q_{ini}^u, q_N^u = q_{ini}^u;
 \end{aligned} \tag{12}$$

In (12), C1 specifies the value ranges of the transmit time factor, the reflection coefficient factors, and the transmit time allocation factors for both BackCom and active transmission. P_{\max}^{UAV} and P_{\max}^{node} in C2 denote the maximum transmit power of the UAV and the IoT nodes, respectively. C3 constrains the total transmit time for both BackCom and active transmission. C4 guarantees the long-term minimum throughput requirement for each IoT node. In C5, the transmit power consumption of each IoT node cannot exceed the remaining harvested energy after BackCom. C6 ensures that the power consumption of each IoT node during BackCom and active transmission should not exceed the energy harvested by the IoT node within θT . C7 constrains the maximum speed of the UAV, V_{\max} , by limiting its flight distance during each time slot. In C8, the UAV is dispatched from an initial location and flies back to the initial location at the end of the first time period.

The formulated problem \mathbf{P}_1 is a non-convex fractional optimization problem with multiple variables coupling in both the objective function and the constraints, i.e., P^u , \mathbf{Z}_n , $\boldsymbol{\tau}_n$, \mathbf{t} , \mathbf{P} and \mathbf{q} . Thus, it would be extremely difficult to solve \mathbf{P}_1 directly. In order to make this optimization problem more tractable, we first determine the optimal transmit power of the UAV, as summarized in Lemma 1.

Lemma 1: In our proposed system model, the optimal transmit power of the UAV for maximizing the total EE of all the IoT nodes is the maximum UAV transmit power, i.e., $P^{u*} = P_{\max}^{\text{UAV}}$, where $*$ denotes the optimal solution.

Proof. Please see Appendix A. ■

Remark 1: Lemma 1 indicates that letting the UAV transmit with the maximum allowed power can maximize the EE of all the ground IoT nodes. For BackCom, since the IoT nodes reflect the incident RF signal from the UAV, the throughput of BackCom improves with higher UAV transmit power without increasing the IoT node's power consumption, thus the EE of IoT nodes increases. For active transmission, the higher UAV transmit power reduces the time for harvesting energy, and the IoT nodes will have more time to transmit information to the reader, thus increasing the throughput and the EE.

B. Problem Transformation

Based on Lemma 1, \mathbf{P}_1 is transformed into

$$\begin{aligned} \mathbf{P}_2 : \quad & \max_{\{\theta, \mathbf{Z}_n, \tau_n, \mathbf{t}, \mathbf{P}, \mathbf{q}\}} \frac{\sum_{i=1}^M \sum_{n=1}^N W \tau_{i,n} \log_2 \left(1 + \frac{\varphi P_{\max}^{\text{uav}} h_{i,n}^u Z_{i,n} h_i^r}{W \sigma^2} \right) + \sum_{i=1}^M W t_i \log_2 \left(1 + \frac{P_i h_i^r}{W \sigma^2} \right)}{\sum_{i=1}^M \sum_{n=1}^N P_{\text{cir}}^B \tau_{i,n} + \sum_{i=1}^M (P_{\text{cir}}^H + P_i) t_i} \\ \text{s.t.} \quad & \text{C1, C3, C4, C6, C7, C8;} \\ & \text{C2-1 : } 0 \leq P_i \leq P_{\max}^{\text{node}}, \forall i; \end{aligned} \quad (13)$$

Next, we employ Dinkelbach's method to transform the fractional objective function into a subtractive form. Letting Q^* denote the maximum EE, based on [28], Q^* can be achieved if and only if the following equation holds:

$$\max_{\{\theta, \mathbf{Z}_n, \tau_n, \mathbf{t}, \mathbf{P}, \mathbf{q}\}} \sum_{i=1}^M \sum_{n=1}^N R_{i,n}^B + \sum_{i=1}^M R_i^H - Q^* EC_{\text{sum}} = \sum_{i=1}^M \sum_{n=1}^N R_{i,n}^{B*} + \sum_{i=1}^M R_i^{H*} - Q^* EC_{\text{sum}}^* = 0. \quad (14)$$

Based on (13), \mathbf{P}_2 is transformed into

$$\begin{aligned} \mathbf{P}_3 : \quad & \max_{\{\theta, \mathbf{Z}_n, \tau_n, \mathbf{t}, \mathbf{P}, \mathbf{q}\}} \sum_{i=1}^M \sum_{n=1}^N R_{i,n}^B + \sum_{i=1}^M R_i^H - Q EC_{\text{sum}} \\ \text{s.t.} \quad & \text{C1, C2-1, C3, C4, C6, C7, C8.} \end{aligned} \quad (15)$$

where Q denotes a small positive value that is used as the initial value of Q^* . Although \mathbf{P}_3 is more tractable than \mathbf{P}_2 , it is still non-convex due to the coupling between \mathbf{Z}_n and τ_n , \mathbf{P} and \mathbf{t} . We solve this coupling issue by introducing the following auxiliary vectors: $\mathbf{X}_n = [X_{1,n}, X_{2,n}, \dots, X_{M,n}]$, $n \in \mathcal{N}$ and $\mathbf{Y} = [Y_1, Y_2, \dots, Y_M]$, where $X_{i,n} = Z_{i,n} \tau_{i,n}$ and $Y_i = P_i t_i$. Then, \mathbf{P}_3 is transformed into

$$\begin{aligned} \mathbf{P}_4 : \quad & \max_{\{\theta, \mathbf{X}_n, \tau_n, \mathbf{t}, \mathbf{Y}, \mathbf{q}\}} \sum_{i=1}^M \sum_{n=1}^N R_{i,n}^{B'} + \sum_{i=1}^M R_i^{H'} - Q EC_{\text{sum}}' \\ \text{s.t.} \quad & \text{C3, C7, C8;} \\ & \text{C1-1 : } 0 \leq \theta \leq 1, \tau_{i,n} \geq 0, \mathbf{t} \geq 0, \forall i, \forall n; \\ & \text{C2-2 : } 0 \leq X_{i,n} \leq \tau_{i,n}, 0 \leq Y_i \leq t_i P_{\max}^{\text{node}}, \forall i, \forall n; \\ & \text{C4-1 : } \sum_{n=1}^N R_{i,n}^{B'} + R_i^{H'} \geq R_{\min}, \forall i, \forall n; \\ & \text{C6-1 : } EH_i' - EC_i' \geq 0, \forall i, \end{aligned} \quad (16)$$

where $R_{i,n}^{B'}$ = $W\tau_{i,n}\log_2\left(1 + \frac{\varphi P_{max}^{uav} X_{i,n} h_{i,n}^u h_i^r}{\tau_{i,n} W \sigma^2}\right)$, $R_i^{H'}$ = $W t_i \log_2\left(1 + \frac{Y_i h_i^r}{t_i W \sigma^2}\right)$, EC_i' = $\sum_{n=1}^N PC^B \tau_{i,n} + (PC^H t_i + Y_i)$, and the total amount of energy harvested by IoT node i during BackCom is rewritten as

$$\begin{aligned} EH_i' &= \sum_{n=1}^N [P_{max}^{uav} \eta h_{i,n}^u (\tau_{i,n} - X_{i,n}) + P_{max}^{uav} \eta h_{i,n}^u (\frac{\theta T}{N} - \tau_{i,n})] \\ &= \sum_{n=1}^N P_{max}^{uav} \eta h_{i,n}^u (\frac{\theta T}{N} - X_{i,n}). \end{aligned} \quad (17)$$

C. Problem Solution

We note that \mathbf{P}_4 is still non-convex and challenging to solve due to the coupling among the UAV trajectory \mathbf{q} , \mathbf{X}_n and τ_n in the objective function, C4-1 and C5-2. To this end, we propose a BCD method to decompose \mathbf{P}_4 into two sub-problems, namely, the optimization of communication resource allocation including θ , \mathbf{X}_n , \mathbf{Y} , τ_n , and \mathbf{t} with fixed UAV trajectory, and the optimization of the UAV trajectory optimization for a given communication resource allocation. Then, we solve \mathbf{P}_4 by solving these two subproblems alternately. This process leads to a Dinkelbach based iterative algorithm given in **Algorithm 1**, which is also illustrated as a flow chart in Fig. 3.

1) *Communication resource allocation optimization*: For a given UAV trajectory \mathbf{q} , the communication resource allocation sub-problem is formulated as

$$\begin{aligned} \mathbf{P}_{4.1} : \quad & \max_{\{\theta, \mathbf{X}_n, \tau_n, \mathbf{Y}, \mathbf{t}\}} \sum_{i=1}^M \sum_{n=1}^N R_{i,n}^{B'} + \sum_{i=1}^M R_i^{H'} - QEC_{sum}' \\ & \text{s.t.} \\ & \text{C1-1, C2-2, C3, C4-1, C6-1.} \end{aligned} \quad (18)$$

It is easy to verify that $\mathbf{P}_{4.1}$ is a standard convex optimization problem. In the following, we will solve this problem by using the Karush-Kuhn-Tucker (KKT) conditions. First, the Lagrangian function for $\mathbf{P}_{4.1}$ is given by

$$\begin{aligned} & \mathbb{L}(\theta, \mathbf{X}_n, \tau_n, \mathbf{Y}, \mathbf{t}, \boldsymbol{\alpha}_n^{(1)}, \boldsymbol{\alpha}^{(2)}, \boldsymbol{\beta}^{(1)}, \beta^{(2)}, \boldsymbol{\gamma}, \boldsymbol{\phi}) \\ &= \sum_{i=1}^M \sum_{n=1}^N W\tau_{i,n} \log_2 \left(1 + \frac{\varphi P_{max}^{uav} h_{i,n}^u X_{i,n} h_i^r}{\tau_{i,n} W \sigma^2} \right) \\ &+ \sum_{i=1}^M W t_i \log_2 \left(1 + \frac{Y_i h_i^r}{t_i W \sigma^2} \right) - Q \left(\sum_{i=1}^M \sum_{n=1}^N PC^B \tau_{i,n} + \sum_{i=1}^M (PC^H t_i + Y_i) \right) \\ &+ \sum_{i=1}^M \sum_{n=1}^N \alpha_{i,n}^{(1)} (\tau_{i,n} - X_{i,n}) + \sum_{i=1}^M \alpha_i^{(2)} (t_i P_{max}^{node} - Y_i) + \sum_{n=1}^N \beta^{(1)} (\frac{\theta T}{N} - \sum_{i=1}^M \tau_{i,n}) \\ &+ \beta^{(2)} \left((1 - \theta)T - \sum_{i=1}^M t_i \right) + \sum_{i=1}^M \gamma_i \left(\sum_{n=1}^N R_{i,n}^{B'} + R_i^{H'} - R_{min} \right) + \sum_{i=1}^M \phi_i (EH_i' - EC_{sum}'), \end{aligned} \quad (19)$$

where $\boldsymbol{\alpha}_n^{(1)} = [\alpha_{1,n}^{(1)}, \alpha_{2,n}^{(1)}, \dots, \alpha_{M,n}^{(1)}] \succeq \mathbf{0}$, $n \in \mathcal{N}$, $\boldsymbol{\alpha}^{(2)} = [\alpha_1^{(2)}, \alpha_2^{(2)}, \dots, \alpha_M^{(2)}] \succeq \mathbf{0}$, $\boldsymbol{\beta}^{(1)} = [\beta_1^{(1)}, \beta_2^{(1)}, \dots, \beta_N^{(1)}] \succeq \mathbf{0}$, $\beta^{(2)} \geq 0$, $\boldsymbol{\gamma} = [\gamma_1, \gamma_2, \dots, \gamma_M] \succeq \mathbf{0}$ and $\boldsymbol{\phi} = [\phi_1, \phi_2, \dots, \phi_M] \succeq \mathbf{0}$ are the Lagrange multipliers associated with C2-2, C3, C4-1 and C5-2, respectively. Please note that the non-negativity constraints in C1-1 and C2-2, i.e., $\theta \geq 0, \tau_{i,n} \geq 0, t_i \geq 0$ and $X_{i,n} \geq 0, Y_i \geq 0$, are considered in the optimal solution in the following. Accordingly, the dual function of $\mathbf{P}_{4.1}$ is denoted by $\mathbb{G}(\boldsymbol{\alpha}_n^{(1)}, \boldsymbol{\alpha}^{(2)}, \boldsymbol{\beta}^{(1)}, \beta^{(2)}, \boldsymbol{\gamma}, \boldsymbol{\phi}) = \max_{\theta, \mathbf{X}_n, \tau_n, \mathbf{Y}, \mathbf{t}} \mathbb{L}(\theta, \mathbf{X}_n, \tau_n, \mathbf{Y}, \mathbf{t})$, and the Lagrangian dual optimization problem can be formulated as

$$\min_{\boldsymbol{\alpha}_n^{(1)}, \boldsymbol{\alpha}^{(2)}, \boldsymbol{\beta}^{(1)}, \beta^{(2)}, \boldsymbol{\gamma}, \boldsymbol{\phi}} \max_{\theta, \mathbf{X}_n, \tau_n, \mathbf{Y}, \mathbf{t}} \mathbb{L}. \quad (20)$$

Since $\mathbf{P}_{4.1}$ is a standard convex optimization problem, it satisfies Slater's condition so that the duality gap between $\mathbf{P}_{4.1}$ and (20) is zero. Thus, we can solve $\mathbf{P}_{4.1}$ by maximizing $\mathbb{L}(\theta, \mathbf{X}_n, \tau_n, \mathbf{Y}, \mathbf{t})$ for given $\alpha_n^{(1)}, \alpha^{(2)}, \beta^{(1)}, \beta^{(2)}, \gamma, \phi$, and minimizing $\mathbb{G}(\alpha_n^{(1)}, \alpha^{(2)}, \beta^{(1)}, \beta^{(2)}, \gamma, \phi)$ for given $\theta, \mathbf{X}_n, \tau_n, \mathbf{Y}, \mathbf{t}$. The details are provided as follows.

For given Lagrange multipliers, based on the KKT conditions, we take the derivative of \mathbb{L} with respect to $X_{i,n}, Y_i, \tau_{i,n}, t_i$ and θ , respectively, yielding

$$\frac{\partial \mathbb{L}}{\partial X_{i,n}} = \frac{W(1+\gamma_i)\log_2 e}{\frac{X_{i,n}}{\tau_{i,n}} + \frac{W\sigma^2}{\varphi P_{\max}^{uav} h_{i,n}^u h_i^r}} - \alpha_{i,n}^{(1)} - \phi_i P_{\max}^{uav} \eta h_{i,n}^u, \quad (21)$$

$$\frac{\partial \mathbb{L}}{\partial Y_i} = \frac{W(1+\gamma_i)\log_2 e}{\frac{Y_i}{t_i} + \frac{W\sigma^2}{h_i^r}} - \alpha_i^{(2)} - Q - \phi_i, \quad (22)$$

$$\frac{\partial \mathbb{L}}{\partial \tau_{i,n}} = W(1+\gamma_i) \left(\log_2 \left(1 + \frac{\varphi P_{\max}^{uav} h_{i,n}^u h_i^r X_{i,n}}{W\sigma^2 \tau_{i,n}} \right) - \frac{\log_2 e}{1 + \frac{W\sigma^2}{\varphi P_{\max}^{uav} h_{i,n}^u h_i^r \frac{X_{i,n}}{\tau_{i,n}}}} \right) - QPC^B + \alpha_{i,n}^{(1)} - \beta_n^{(1)} - \phi_i PC^B, \quad (23)$$

$$\frac{\partial \mathbb{L}}{\partial t_i} = W(1+\gamma_i) \left(\log_2 \left(1 + \frac{h_i^r Y_i}{W\sigma^2 t_i} \right) - \frac{\log_2 e}{1 + \frac{W\sigma^2}{h_i^r \frac{Y_i}{t_i}}} \right) - QPC^H + \alpha_i^{(2)} P_{\max}^{node} - \beta^{(2)} - \phi_i PC^H, \quad (24)$$

$$\frac{\partial \mathbb{L}}{\partial \theta} = \sum_{n=1}^N \beta_n^{(1)} \frac{T}{N} - \beta^{(2)} T + \sum_{i=1}^M \sum_{n=1}^N \phi_i P_{\max}^{uav} \eta h_{i,n}^u \frac{T}{N}. \quad (25)$$

By letting (21) and (22) equal to 0, we obtain

$$Z_{i,n}^* = \frac{X_{i,n}}{\tau_{i,n}} = \min \left(1, W \left[\frac{(1+\gamma_i)\log_2 e}{\alpha_{i,n}^{(1)} + \phi_i P_{\max}^{uav} \eta h_{i,n}^u} - \frac{\sigma^2}{\varphi P_{\max}^{uav} h_{i,n}^u h_i^r} \right]^+ \right), \quad (26)$$

$$P_i^* = \frac{Y_i}{t_i} = \min \left(P_{\max}^{node}, W \left[\frac{(1+\gamma_i)\log_2 e}{\alpha_i^{(2)} + Q + \phi_i} - \frac{\sigma^2}{h_i^r} \right]^+ \right), \quad (27)$$

where $Z_{i,n}^*$ and P_i^* denote the optimal reflection coefficient of IoT node i at time slot n during BackCom and the optimal transmit power of IoT node i during active transmission, respectively, and $[x]^+ \triangleq \max\{x, 0\}$.

Remark 2: From (26), we find that $Z_{i,n}^*$ increases with higher h_i^r , indicating that an IoT node closer to the reader uses a higher reflection coefficient to backscatter information. The reason is that the UAV can afford to backscatter a higher portion of the incident RF signal power for achieving a higher EE, given that its circuit power consumption for BackCom is constant. From (27), we can see that P_i^* increases with h_i^r , which is the channel gain from IoT node i to the reader. That is, an IoT node with a better channel to the reader should transmit with higher power during active transmission. The resulting higher throughput will overweight the increased power consumption and lead to a higher EE.

Based on (25) and substituting (26) and (27) into (23) and (24), respectively, we find that the Lagrangian function \mathbb{L} is linear with respect to $\tau_{i,n}, t_i$ and θ . This indicates that the optimal values of $\tau_{i,n}, t_i$ and θ can be found at

the vertices of the feasible region. By substituting (26), (27) into $\mathbf{P}_{4.1}$ and after some manipulations, we obtain an equivalent optimization problem as follows,

$$\begin{aligned} & \max_{\theta, \tau_n, \mathbf{t}} \sum_{i=1}^M \sum_{n=1}^N W \tau_{i,n} \left(\log_2 \left(1 + \frac{\varphi P_{\max}^{uav} h_{i,n}^u h_i^r Z_{i,n}^*}{W \sigma^2} \right) - Q P C^B \right) + \sum_{i=1}^M W t_i \left(\log_2 \left(1 + \frac{h_i^r P_i^*}{W \sigma^2} \right) - Q (P_i^* + P C^H) \right) \\ & \text{s.t.} \\ & \text{C1-1, C3;} \\ & \text{C4-2: } \sum_{n=1}^N R_{i,n}^{B''} + R_i^{H''} \geq R_{\min}, \forall i; \\ & \text{C6-2: } E H_i'' - E C_i'' \geq 0, \forall i, \end{aligned} \tag{28}$$

where $R_{i,n}^{B''} = W \tau_{i,n} \log_2 \left(1 + \frac{\varphi P_{\max}^{uav} h_{i,n}^u h_i^r Z_{i,n}^*}{W \sigma^2} \right)$, $R_i^{H''} = W t_i \log_2 \left(1 + \frac{h_i^r P_i^*}{W \sigma^2} \right)$, $E H_i'' = P^u \eta h_{i,n}^u \left(\frac{\theta T}{N} - \tau_{i,n} Z_{i,n}^* \right)$, and $E C_i'' = \sum_{n=1}^N P C^B \tau_{i,n} + (P C^H + P_i^*) t_i$.

It is obvious that problem (28) is a linear programming problem with respect to $\tau_{i,n}, t_i$ and θ . Thus, we can solve problem (28) efficiently by using standard convex optimization tools, e.g., CVX. Then, $X_{i,n}$ and Y_i can be obtained by substituting $\tau_{i,n}$ and t_i back into (26) and (27), respectively.

Remark 3: In (28), the objective function is the weighted sum of $\tau_{i,n}$ and t_i . Thus, the maximum EE of all the ground IoT nodes can be achieved by allowing the IoT nodes to use up all the available time, i.e., T , for BackCom and active transmission. Furthermore, in order to maximize the EE, more time for BackCom and active transmission should be allocated to the IoT nodes with better channel conditions from themselves to the UAV and to the reader. For those IoT nodes whose channel conditions are not good enough to allow for EE improvement, the time allocated to them will guarantee that they can achieve their minimum throughput requirement. The above remark will be verified in Section V.

Since the dual optimization problem in (20) is convex as is $\mathbf{P}_{4.1}$, for given $\tau_{i,n}, t_i$ and θ , we use a gradient based method to update the Lagrange multipliers $\alpha_n^{(1)}, \alpha_n^{(2)}, \beta^{(1)}, \beta^{(2)}, \gamma, \phi$ as follows,

$$\alpha_{i,n}^{(1)}(l+1) = \left[\alpha_{i,n}^{(1)}(l) - s_1 (\tau_{i,n} - X_{i,n}) \right]^+, \forall i, \forall n; \tag{29}$$

$$\alpha_i^{(2)}(l+1) = \left[\alpha_i^{(2)}(l) - s_2 (t_i P_{\max}^{node} - Y_i) \right]^+, \forall i; \tag{30}$$

$$\beta_n^{(1)}(l+1) = \left[\beta_n^{(1)}(l) - s_3 \left(\frac{\theta T}{N} - \sum_{i=1}^M \tau_{i,n} \right) \right]^+, \forall n; \tag{31}$$

$$\beta^{(2)}(l+1) = \left[\beta^{(2)}(l) - s_4 \left((1-\theta)T - \sum_{i=1}^M t_i \right) \right]^+; \tag{32}$$

$$\gamma_i(l+1) = \left[\gamma_i(l) - s_5 \left(\sum_{n=1}^N R_{i,n}^{B'} + R_i^{H'} - R_{\min} \right) \right]^+, \forall i; \tag{33}$$

$$\phi_i(l+1) = \left[\phi_i(l) - s_6(EH_i' - EC_{sum}') \right]^+, \forall i, \quad (34)$$

where l is the iteration index for updating the Lagrange multipliers, s_1, s_2, s_3, s_4, s_5 and s_6 are the step sizes for the associated Lagrange multipliers. How to choose the values of the step sizes in a gradient method has been discussed in [29] and is thus omitted here for brevity. Then, we use the updated Lagrange multipliers to update $\tau_{i,n}, t_i$ and θ in problem (28).

2) *UAV trajectory optimization*: For given communication resource allocation in terms of $X_{i,n}, Y_i, \tau_{i,n}, t_i$ and θ , the UAV trajectory optimization sub-problem is formulated as

$$\begin{aligned} \mathbf{P}_{4.2} : \max_{\{\mathbf{q}\}} & \sum_{i=1}^M \sum_{n=1}^N R_{i,n}^{B'} + \sum_{i=1}^M R_i^{H'} - QEC_{sum}' \\ \text{s.t.} & \\ & \text{C4-1, C6-1, C7, C8.} \end{aligned} \quad (35)$$

$\mathbf{P}_{4.2}$ is still non-convex due to the non-convex vectors \mathbf{q} in the objective function and the constraints. An SCP based technique is employed to obtain a locally optimal solution by successively maximizing a lower bound of the objective function in an iterative manner. Specifically, let $\mathbf{q}^0 = [q_1^0, q_2^0, \dots, q_N^0]$ denote the initial UAV trajectory and $\mathbf{q}^{l'} = [q_1^{l'}, q_2^{l'}, \dots, q_N^{l'}]$ denote the obtained UAV trajectory after the l' th iteration. Accordingly, we propose the following lemma to transform $R_{i,n}^{B'}$ and EH_i' into convex formulations [15], [16], [30].

Lemma 2: For any given $\mathbf{q}^{l'}, l' \geq 0$, we have

$$R_{i,n}^{B'}(\mathbf{q}) \geq R_{i,n}^{B'}(\mathbf{q}^{l'}), \forall i, \forall n; \quad (36)$$

$$EH_i'(\mathbf{q}) \geq EH_i'(\mathbf{q}^{l'}), \forall i, \quad (37)$$

where

$$R_{i,n}^{B'}(\mathbf{q}^{l'}) = W\tau_{i,n} \log_2 \left(1 + \frac{\varphi P_{\max}^{uav} h_i^r X_{i,n} \beta_0 \mu}{W\sigma^2 \tau_{i,n} (H^2 + F_0)} \right) - \frac{W\tau_{i,n} \log_2 e}{\left(1 + \frac{W\sigma^2 \tau_{i,n} (H^2 + F_0)}{\varphi P_{\max}^{uav} h_i^r X_{i,n} \beta_0 \mu} \right) (H^2 + F_0)} (F - F_0), \forall i, \forall n, \quad (38)$$

$$EH_i'(\mathbf{q}^{l'}) = \frac{P_{\max}^{uav} \eta \beta_0 \mu \left(\frac{\theta T}{N} - X_{i,n} \right)}{H^2 + F_0} - \frac{P_{\max}^{uav} \eta \beta_0 \mu \left(\frac{\theta T}{N} - X_{i,n} \right)}{(H^2 + F_0)^2} (F - F_0), \forall i, \forall n, \quad (39)$$

$$F = \|q_n^{l'} - q_i^g\|^2, F_0 = \|q_n^0 - q_i^g\|^2, \forall i, \forall n, \quad (40)$$

the equations in (36) and (37) only hold when $\mathbf{q}^0 = \mathbf{q}^{l'}$.

Proof. Please see Appendix B. ■

Based on Lemma 2, we optimize the UAV trajectory \mathbf{q} by replacing $R_{i,n}^{B'}$ and EH_i' in $\mathbf{P}_{4.2}$ with their respective lower bounds $R_{i,n}^{B'}(\mathbf{q}^l)$ and $EH_i'(\mathbf{q}^l)$ in (38) and (39) at each iteration l' . By substituting (38) and (39) into problem (35), $\mathbf{P}_{4.2}$ can be equivalently formulated as

$$\begin{aligned} \mathbf{q}^* &= \arg \max_{\{\mathbf{q}^l\}} \sum_{i=1}^M \sum_{n=1}^N R_{i,n}^{B'}(\mathbf{q}^l) + \sum_{i=1}^M R_i^{H'} - QEC_{sum}' \\ \text{s.t.} & \\ & \text{C4-1, C7, C8,} \\ & \text{C6-3 : } EH_i'(\mathbf{q}^l) - EC_i' \geq 0, \forall i. \end{aligned} \quad (41)$$

Since (38) and (39) are convex with respect to \mathbf{q}^l , problem (41) is a convex optimization problem and can be efficiently solved by using standard convex optimization methods, e.g., the interior point method, which is omitted here for brevity.

Remark 4: The factor ' $F - F_0$ ' in (39) indicates that a higher amount of energy can be harvested when the UAV is closer to the IoT nodes, as the received power will be higher. In order to maximize the objective function of (41), which is equivalent to maximizing the total EE of all the ground IoT nodes, the UAV needs to be closer to the IoT nodes that can achieve a higher throughput than the other IoT nodes during BackCom. Meanwhile, the time allocation for BackCom and active transmission will guarantee the minimum throughput requirements for all IoT nodes. That is to say, the IoT nodes allocated less time during BackCom will have enough time to transmit information actively to meet the minimum throughput requirement during active transmission. The above remark will be verified in Section V.

D. Dinkelbach-Based Iterative Algorithm

We propose a Dinkelbach-based iterative algorithm in Algorithm 1 to summarize the optimization process in Section III-C.

In Algorithm 1, k is the iteration index for updating Q , i.e., the maximum EE, and ϵ is set to control the convergence of the objective function in \mathbf{P}_4 . The flow chart of Algorithm 1 is illustrated in Fig. 3.

IV. CONVERGENCE AND COMPUTATIONAL COMPLEXITY ANALYSIS

We first analyze the convergence of Algorithm 1, which includes two layers of iteration, where the two inner layer iterative loops aim to achieve the convergence of Lagrange multipliers for solving $\mathbf{P}_{4.1}$ and the convergence of the UAV's trajectory, respectively, and the outer layer iteration seeks the convergence of the BCD algorithm that decomposes \mathbf{P}_4 into $\mathbf{P}_{4.1}$ and $\mathbf{P}_{4.2}$. Since $\mathbf{P}_{4.1}$ is a standard convex optimization problem, the iterative updates of θ, τ, \mathbf{t} and the Lagrange multipliers $\alpha_n^{(1)}, \alpha_n^{(2)}, \beta^{(1)}, \beta^{(2)}, \gamma, \phi$ are guaranteed to converge to the optimal solution of $\mathbf{P}_{4.1}$. To solve $\mathbf{P}_{4.2}$, successive convex programming (SCP) method is used. We denote the maximum EE obtained by solving $\mathbf{P}_{4.2}$ in the $(l+1)$ th iteration by $EE(l+1)$, and denote the maximum EE obtained through solving (41) in the l th and the $(l+1)$ th iteration by $EE_{lb}(l)$ and $EE_{lb}(l+1)$, respectively. Based on [30], we have

$$EE_{lb}(l) \leq EE_{lb}(l+1), \quad (42)$$

Algorithm 1 Dinkelbach based iterative algorithm

Input: \mathcal{M}, \mathcal{N} .

Output: $Q^*, \mathbf{Z}_n^*, \boldsymbol{\tau}_n^*, \mathbf{t}^*, \mathbf{P}^*, \mathbf{q}^*$.

Initialize: $k = 1, Q(k) = Q(0), \epsilon$.

- 1: **repeat**
 - 2: Initialize \mathbf{q} ;
 - 3: **repeat**
 - 4: **repeat**
 - 5: Initialize $\boldsymbol{\alpha}_n^{(1)}, \boldsymbol{\alpha}^{(2)}, \boldsymbol{\beta}^{(1)}, \beta^{(2)}, \gamma, \phi$;
 - 6: Obtain $\theta, \mathbf{X}_n, \boldsymbol{\tau}_n, \mathbf{Y}, \mathbf{t}$ by solving $\mathbf{P}_{4.1}$;
 - 7: Update the Lagrange multipliers $\boldsymbol{\alpha}_n^{(1)}, \boldsymbol{\alpha}^{(2)}, \boldsymbol{\beta}^{(1)}, \beta^{(2)}, \gamma, \phi$ in (28)-(33), respectively;
 - 8: **until** $\boldsymbol{\alpha}_n^{(1)}, \boldsymbol{\alpha}^{(2)}, \boldsymbol{\beta}^{(1)}, \beta^{(2)}, \gamma, \phi$ converge;
 - 9: **repeat**
 - 10: Initialize \mathbf{q}^0 ;
 - 11: Obtain \mathbf{q}^* by solving $\mathbf{P}_{4.2}$;
 - 12: Update the obtained UAV trajectory \mathbf{q}^l ;
 - 13: **until** \mathbf{q}^* converges;
 - 14: **until** $\boldsymbol{\alpha}_n^{(1)}, \boldsymbol{\alpha}^{(2)}, \boldsymbol{\beta}^{(1)}, \beta^{(2)}, \gamma, \phi$ and \mathbf{q} converge after $k = 2$;
 - 15: Compute $R_{i,n}^B, R_i^H$ and EC_{sum} in (6), (7) and (9), respectively;
 - 16: $k = k + 1$;
 - 17: Update $Q(k) = \frac{R_{sum}}{EC_{sum}}$;
 - 18: **until** $|\min_{i \in M, m \in N} \sum_{i=1}^M \sum_{n=1}^N R_{i,n}^B + \sum_{i=1}^M R_i^H - Q(k)EC_{sum}| \leq \epsilon$.
-

$$EE_{lb}(l+1) \leq EE(l+1), \quad (43)$$

where l is the iteration number, (42) holds since $EE_{lb}(l+1)$ is the optimal solution of (41), and (43) holds since a convex function is globally lower bounded by its first-order Taylor expansion. The inequalities in (42) and (43) imply that the achieved maximal EE is non-decreasing after each iteration and is upper bounded, and the approximate problem (41) of $\mathbf{P}_{4.2}$ is solved optimally locally in each iteration. Therefore, the SCP based method for solving $\mathbf{P}_{4.2}$ is guaranteed to converge to a locally optimal solution. After each iteration of the BCD algorithm that alternately solves $\mathbf{P}_{4.1}$ and $\mathbf{P}_{4.2}$, the objective function value of \mathbf{P}_4 is nondecreasing with updated variables. Meanwhile, \mathbf{P}_4 is also upper bounded by its associated constraints, thus the BCD algorithm is guaranteed to converge to a solution of \mathbf{P}_4 .

Next, we evaluate the computational complexity of Algorithm 1. The computational complexity of the Lagrange dual method in (19) for solving $\mathbf{P}_{4.1}$ is $\mathcal{O}(\Delta_1 MN)$ [31], where Δ_1 is the number of iterations for updating the

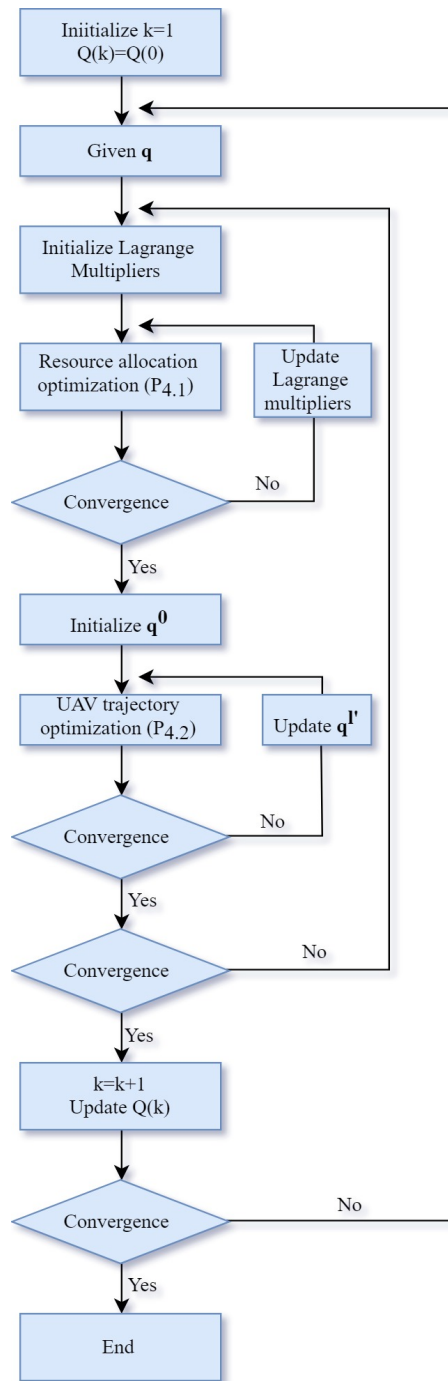


Fig. 3: Flow chart of **Algorithm 1**.

Lagrange multipliers. The interior point method used to solve problem (41) has a computational complexity of $\mathcal{O}(\sqrt{C}\frac{1}{\zeta})$ for each iteration, where C denotes the number of variables, i.e., $C = N$ in (41), and ζ represents the iterative accuracy [29], [32]. The iterations needed for the convergence of the BCD algorithm and Q^* are denoted by Δ_2 and Δ_3 , respectively. Thus, the total computational complexity of Algorithm 1 is $\mathcal{O}[(\Delta_1 MN + \sqrt{C}\frac{1}{\zeta})\Delta_2\Delta_3]$. According to our simulations, the values of Δ_1 , Δ_2 and Δ_3 are in the ranges of 2-5, 2-4 and 3-5, respectively.

V. SIMULATION RESULTS

In this section, we present simulation results to evaluate the time allocation, the UAV trajectory, the convergence of Algorithm 1, and the EE performance versus different parameters based on our proposed Algorithm 1, in comparison with the benchmark schemes, i.e., the UAV-enabled BackCom scheme, the UAV-enabled HTT scheme, the energy consumption minimization scheme, and the fixed PB based hybrid BackCom-HTT scheme. The details of the benchmark schemes are provided in Appendix C. We consider a network, where all the IoT nodes are located within a 2-D region of $10 \times 10 \text{ m}^2$ [33], the UAV's original position and the location of the reader are respectively 10 m and 30 m away from the center of this region, which is set as the origin of the 2D ground plane. The values of the other fixed system parameters are listed in Table 1 [14], [15], [25], [34].

Table 1 Simulation Parameters

Simulation parameter	Value
Number of IoT nodes M	5
Number of time slots N	50
Altitude of UAV H	10m
Maximum speed of UAV V_{max}	10m/s
Coordinate of UAV's original location	(-10,0)
Coordinate of reader location	(30,0)
Channel bandwidth W	10 kHz
Noise power spectral density σ^2	-130 dBm/Hz
Channel power gain at reference distance β_0	-30 dB
Rician factor	7 dB
Pathloss exponent of UAV-node channel	2
Pathloss exponent of node-reader channel	3
Maximum UAV transmit power P_{max}^{uav}	40 dBm
Maximum IoT node transmit power P_{max}^{node}	23 dBm
Energy conversion efficiency η	0.5
Backscatter circuit power consumption P_{cir}^B	200 μw
HTT circuit power consumption P_{cir}^H	1 mw

A. Time Allocation Versus Backscatter Performance Gap

Fig. 4 illustrates the impact of backscatter performance gap φ on the time allocation for BackCom, i.e., θ . It is easy to verify that θ is always 1 for the UAV-enabled backscatter scheme since it only includes BackCom. For the UAV-enabled HTT scheme, θ keeps the same value as 0.28 with different φ , this is also easy to verify that during BackCom in the UAV-enabled HTT scheme, the IoT nodes only harvest energy and then transmit information to the reader during active transmission. For our proposed Algorithm 1, when φ is smaller than -50 dB, θ is the same as that in the UAV-enabled HTT scheme, since the EE provided by BackCom is too low and the minimum throughput requirement R_{min} cannot be met in this case. Same as in the UAV-enabled HTT, the IoT nodes only harvest energy

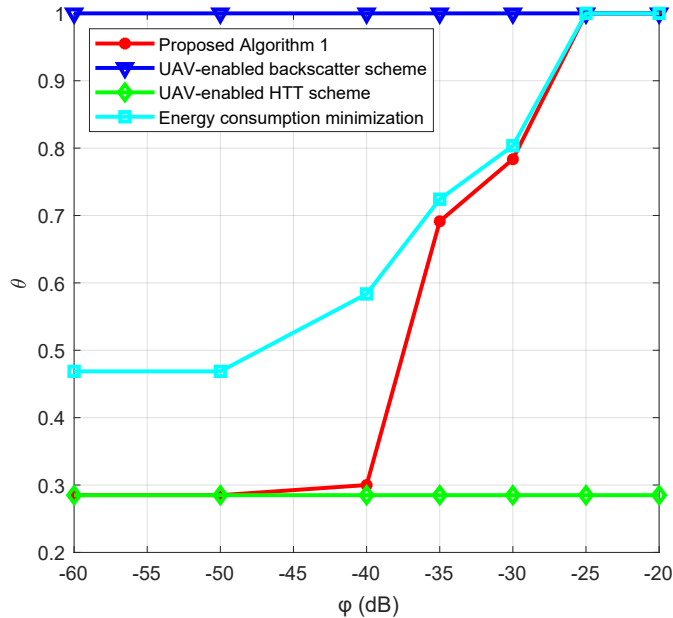


Fig. 4: Portion of time allocated for BackCom versus BackCom performance gap ($R_{min} = 5 \times 10^4$ bit/s).

during BackCom and transmit information to the reader during active transmission. θ slightly increases with the improvement of φ from -50 dB to -40 dB, then it dramatically increases when φ is greater than -40 dB. This is because that BackCom of some IoT nodes at some time slots can gain more EE with higher φ so that more time is allocated to BackCom. It also indicates that θ is sensitive to φ , where θ improves dramatically after exceeding -40 dB. When φ is bigger than -25 dB, θ is always one, which indicates that BackCom dominates the over all time period, and the active transmission of any IoT node at any time slot cannot provide higher EE than that in BackCom.

Comparing the energy consumption minimization scheme with our proposed Algorithm 1, θ in energy consumption minimization scheme is no smaller than that in our proposed Algorithm 1. This is because BackCom consumes much less energy than active transmission due to the low backscatter circuit consumption without transmit power consumption. Specifically, when φ is smaller than -50 dB, the throughput requirement cannot be met by BackCom. Thus, the IoT nodes only harvest energy during BackCom, and transmit information during active transmission. However, in order to minimize the energy consumption, more time is allocated to BackCom for energy harvesting but without energy consumption, since the throughput of all the IoT nodes only need to equal to R_{min} . θ significantly increases from 0.48 to 0.8 with φ increasing from -50 dB -30 dB, which indicates that more time is allocated to BackCom for saving energy while satisfying R_{min} with active transmission. Also, the gap between our proposed Algorithm 1 and the energy consumption minimization scheme becomes smaller since higher φ can both improve the EE and minimize the energy consumption. After φ exceeds -25 dB, the BackCom dominate the over all time period as in our proposed Algorithm 1. We can also see that the EE of each scheme stays constant when φ is less than -50 dB or more than -25 dB.

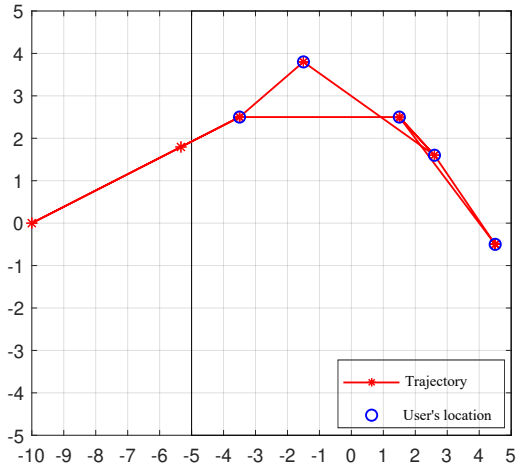


Fig. 5(a): UAV trajectory for a UAV-enabled backscatter network ($\theta = 1$, $R_{min} = 5 \times 10^4$ bit/s).

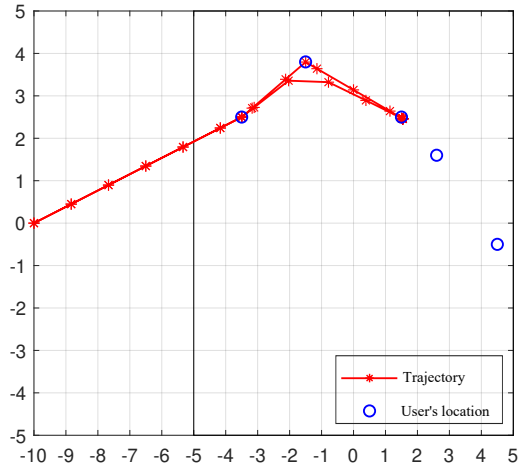


Fig. 5(b): UAV trajectory for a UAV-enabled HTT network ($\theta = 0.27$, $R_{min} = 5 \times 10^4$ bit/s).

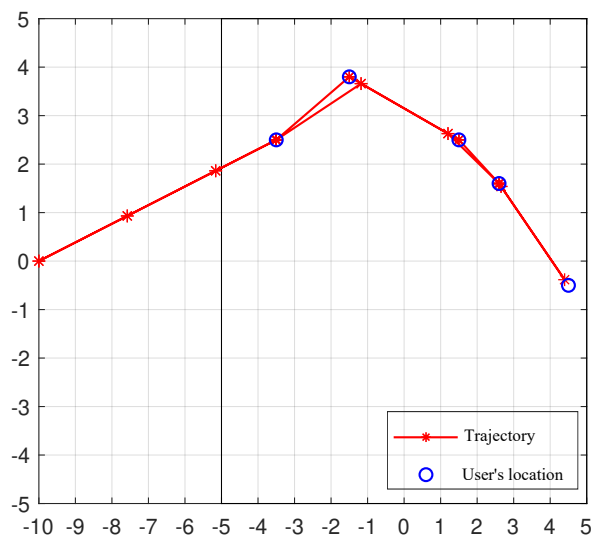


Fig. 5(c): UAV trajectory for a UAV-enabled hybrid network ($\theta = 0.52$, $R_{min} = 5 \times 10^4$ bit/s).

B. UAV Trajectory

In Fig. 5 (a), the UAV trajectory is illustrated for $\theta = 1$, which means that BackCom dominates the whole time block. The UAV is dispatched from the left-most point of the trajectory to provide energy for the IoT nodes, and then flies back to the initial location at the end of the BackCom time period. As we can see, the UAV flies to and hovers above each IoT node to make sure that all the IoT nodes meet R_{min} . Meanwhile, our simulation result shows that the UAV spends the longest time hovering above the right-most IoT node, which helps this IoT node achieve the highest throughput, i.e., 2.79×10^5 bit/s, because it is closest to the reader and can contribute most to the sum EE of all the IoT nodes.

In Fig. 5 (b), the UAV trajectory is illustrated for $\theta = 0.27$, which means that HTT dominates the whole time block. The UAV in this case only flies to and hovers above three IoT nodes and spends the most time hovering above the IoT node at the middle position of all the IoT nodes. This is because the throughput of each IoT node is achieved only via active transmission, which requires sufficient energy harvested during BackCom. Thus, the UAV needs to hover over a position that each IoT node can harvest enough energy for active transmission to meet the throughput requirements. Our simulation result shows that more time for active transmission is allocated to the two IoT nodes that are closer to the reader for achieving higher throughput and sum EE, while the other IoT nodes maintaining the minimum required throughput.

Fig. 5 (c) shows the UAV trajectory for $\theta = 0.52$, which represents a hybrid BackCom-HTT network. We can see that the UAV trajectory is similar to that in Fig. 5 (a), but in the case of Fig. 5(c), the UAV spends less time hovering above the IoT node that is closest to the reader and the other IoT nodes achieve higher throughput with a longer BackCom transmission time. This is because the maximum EE of all the IoT nodes is achieved when the IoT node closest to the reader is allocated the most time for active transmission while the other IoT nodes maintaining the minimum required throughput during the whole time block. Thus, more time for BackCom is allocated to the other IoT nodes for meeting the throughput requirements.

Based on the above results and **Remark 4**, we summarize the insights into the UAV trajectory as follows. First, the UAV tends to fly to the IoT nodes that are closer to the reader, and such IoT nodes can achieve higher throughput and contribute more toward a higher EE of all the IoT nodes. Second, if BackCom dominates the network, the UAV will fly above each IoT node to ensure that all the IoT nodes satisfy the throughput requirement, and the IoT node that is closest to the reader is allocated the most time of BackCom for maximizing the EE of all the IoT nodes. Third, if HTT dominates the network, the UAV spends the most time hovering above the IoT node that is around the middle position of all the IoT nodes, but more time for active transmission is allocated to the IoT nodes closer to the reader for a higher total EE. Fourth, in the case of hybrid backscatter-HTT, the UAV trajectory is similar to that in case of pure BackCom, but the UAV spends less time hovering above the IoT node closest to the reader so that the other IoT nodes may have a longer BackCom time to meet their throughput requirements. Fifth, if the reader's location is changed, the UAV will fly to the IoT nodes that are closer to the updated location of the reader. Last but not least, if the time block is long enough, the UAV trajectory in the above three cases will be a straight line from the initial location to the IoT node closest to the reader for maximizing the total EE, since the throughput requirements of all the other IoT nodes can be satisfied through BackCom or HTT for a sufficiently long time.

C. Convergence of Algorithm 1

Fig. 6 illustrates the convergence of our proposed Algorithm 1 versus different maximum UAV transmit power. It can be observed that our proposed algorithm always converges to the optimal EE after 4_{th} step under any given UAV transmit power. This proves that our proposed Algorithm 1 is computationally efficient. Also, based on Lemma

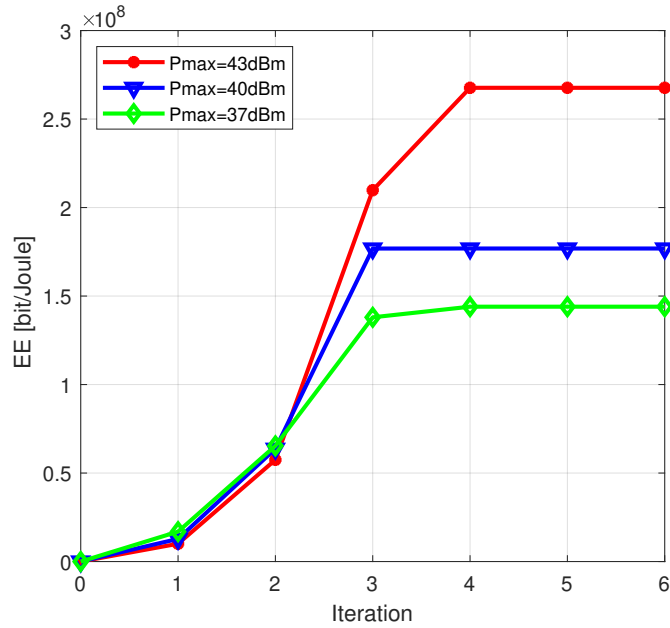


Fig. 6: Convergence of Algorithm 1 ($R_{min} = 5 \times 10^4$ bit/s, $\varphi = -30$ dB)

1, where maximum UAV transmit power is proved to be the optimal value for maximum EE. We can see that higher maximum UAV transmit power achieve higher EE than other cases with lower UAV transmit power in Fig. 6.

D. Total EE Performance

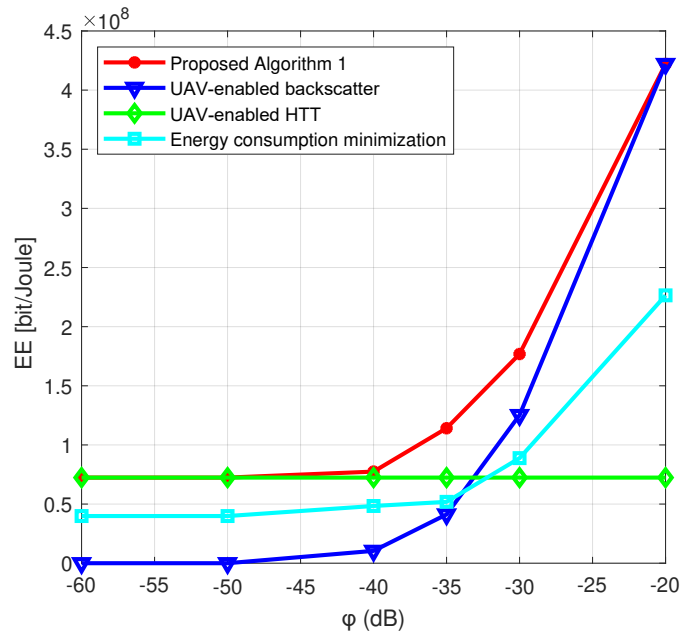


Fig. 7: Total EE versus BackCom performance gap φ ($R_{min} = 5 \times 10^4$ bit/s).

1) *Total EE versus φ* : Fig. 7 illustrates the total EE of all the IoT nodes versus φ . We can see that the total EE of our proposed Algorithm 1 outperforms all other schemes. Next, we describe and explain each curve of each scheme as follows. Firstly, the total EE of UAV-enabled HTT scheme is constant, i.e., 7.2×10^7 bits/s, since the IoT nodes during the first time period in the UAV-enabled HTT scheme only harvest energy, and then transmit information to the reader during active transmission. Thus, the backscatter performance gap of BackCom has no impact on the UAV-enabled HTT scheme. Secondly, the EE of our proposed algorithm is constant when φ is smaller than -40 dB since the IoT nodes under this condition are the same as the IoT nodes in the UAV-enabled HTT scheme in order to meet R_{min} . Then the total EE of our proposed algorithm increases sharply when φ improves from -40 to -20 dB, which indicates that BackCom provide much more EE than active transmission with low φ .

In addition, the total EE of the energy consumption minimization scheme is still constant when φ is smaller than -40 dB due to the same reason explained above, then it gradually increase with the improvement of φ . Also, the total EE of the energy consumption minimization scheme exceeds that of the UAV-enabled HTT scheme after φ is greater than -35 dB due to the longer time allocated to BackCom for saving energy. This also indicates that BackCom can provide more EE with higher φ . The EE of the UAV-enabled backscatter scheme is 0 when φ is smaller than -40 dB, this is because that the IoT nodes cannot meet R_{min} , which fails to contribute EE. When φ increases beyond -20 dB, the total EE of the UAV-enabled backscatter scheme becomes the same as that of our proposed algorithm. This is because BackCom occupies the entire time block in our proposed algorithm when φ is greater than -20 dB. Furthermore, the EE of each scheme will increase with the minimum throughput requirement below the value of 3×10^4 .

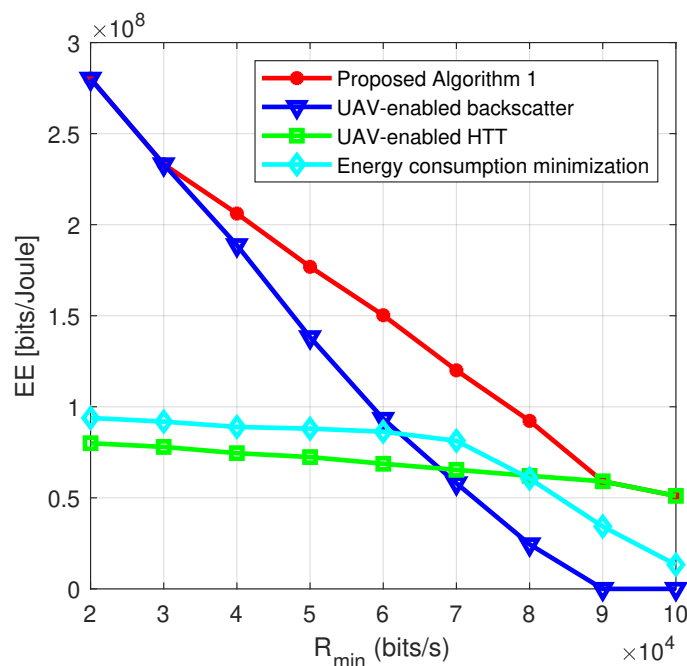


Fig. 8: Total EE versus minimum throughput requirement R_{min} ($\varphi = -30$ dB).

2) *Total EE versus R_{min}* : Fig. 8 plots the total EE of all the IoT nodes versus R_{min} . The total EE of our proposed Algorithm 1 still outperforms that of other schemes. Similarly, the total EE of all schemes decreases with higher R_{min} , since a higher R_{min} makes some IoT nodes at some time slots fail to perform BackCom which greatly decreases the EE. Also, the EE improvement due to a higher throughput cannot compensate for the loss of EE caused by the high energy consumption for meeting a higher throughput requirement. As we can see the total EE of our proposed algorithm significantly decreases but the decreasing rate becomes smaller with the improvement of R_{min} , this is because that more IoT nodes or more time slots are allocated for active transmission, and the EE loss during active transmission is only caused by a higher energy consumption which is smaller than the EE loss due to the low time allocation to BackCom. For the UAV-enabled backscatter scheme, the total EE drops sharply with higher R_{min} , since some IoT nodes cannot meet R_{min} and fail to join the network. Thus, the total EE drops to 0 when R_{min} is too high, e.g., 9×10^4 bits/s. The total EE of our proposed Algorithm 1 and that of the UAV-enabled backscatter scheme are the same when R_{min} is smaller than 3×10^4 bits/s, because BackCom occupies the whole time block for such low R_{min} . When R_{min} is larger than 3×10^4 bits/s, the proposed Algorithm 1 achieves the highest EE among the four considered schemes. As R_{min} further increases, the EE achieved by Algorithm 1 gradually reduces to be the same as that of the UAV-enabled HTT scheme. This is because for very high values of R_{min} , active transmission occupies the whole time block.

The total EE of the UAV-enabled HTT scheme reduces steadily with increasing R_{min} , since the EE loss is only caused by the high energy consumption for meeting a higher throughput requirement. However, the total EE did improve due to higher throughput, thus, the total EE of the UAV-enabled HTT scheme decreases steadily. For the energy consumption minimization scheme, the total EE is around 8.7×10^8 bits/Joule from 3×10^4 bits/s to 6×10^4 bits/s, and then suddenly drops to 2.8×10^7 bits/Joule at $R_{min} = 9 \times 10^4$ bits/s. Since the time allocated to BackCom is more than that allocated to active transmission, the EE obtained by this scheme decreases slowly. After R_{min} exceeds 6×10^4 bits/s, active transmission takes a longer time, and the sudden decreasing of the total EE is due to a much higher energy consumption during active transmission.

3) *Total EE versus V_{max}* : Fig. 9 shows the total EE of all the IoT nodes versus the maximum UAV flying speed V_{max} . It is obvious that the total EE of all the schemes shows the same trend, where our proposed Algorithm 1 achieves the highest EE. Specifically, the total EE of all the schemes gradually increases with higher V_{max} and converges to a certain value after V_{max} exceeds 40 m/s. The reason for that is a higher V_{max} allows the UAV to quickly fly to and stay at some positions which can lead to higher EE while satisfying the constraints, e.g., R_{min} , the amount of energy harvested requirement. Thus, the total EE improves with better UAV trajectory. However, the EE improvement is not large as compared to fig. 7 and fig. 8, this is because V_{max} can only change the optimal trajectory, where the network size is small. Since the UAV can easily travel around a small network, it will not contribute too much EE improvement. Also, the optimal UAV trajectory is constant after V_{max} exceeds 40 m/s, which indicates that the UAV has enough speed to make an optimal trajectory. Thus, the total EE of all the schemes converges after the optimal UAV trajectory is fixed.

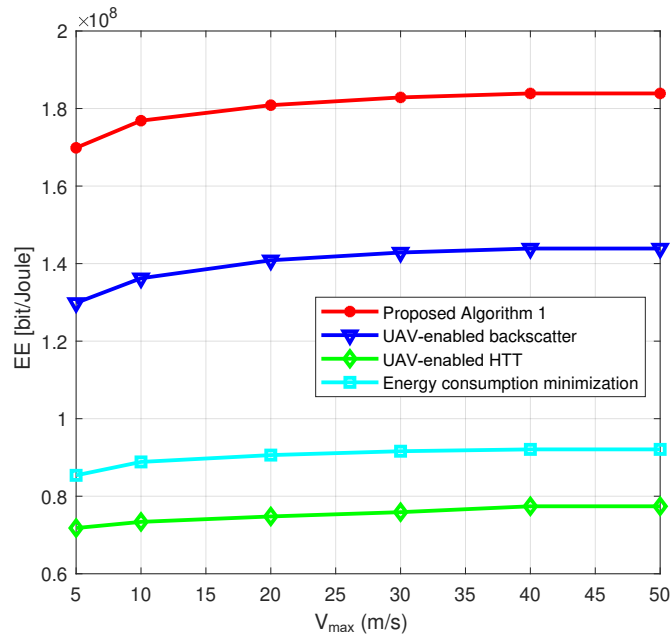


Fig. 9: Total EE versus maximum UAV speed V_{max} ($R_{min} = 5 \times 10^4$ bit/s, $\varphi = -30$ dB).

Same reasons can be explained for the total EE of energy consumption minimization scheme despite this scheme aims to minimize the energy consumption. In addition, the total EE of the UAV-enabled backscatter scheme does not drop like in fig. 7 and fig. 8, this is easy to be verified, the serious drop of the EE for the UAV-enabled backscatter scheme is that the IoT nodes cannot meet R_{min} . However, the IoT node can easily meet R_{min} with high UAV speed.

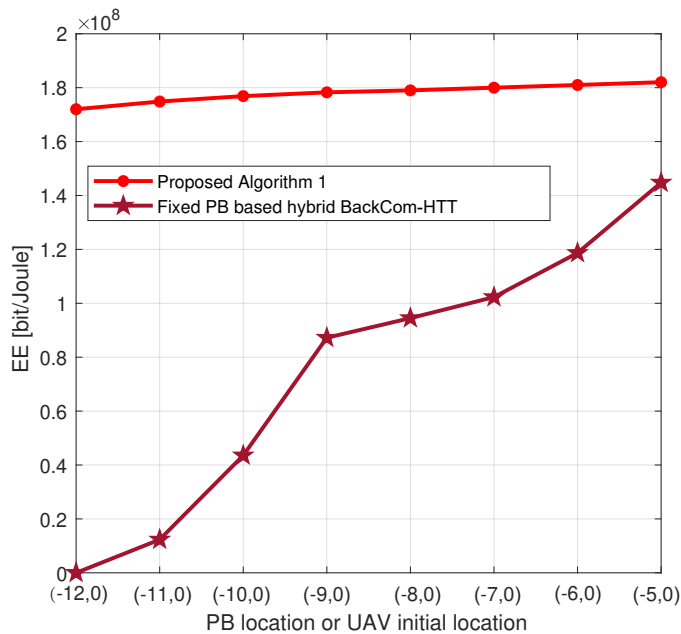


Fig. 10: Total EE versus fixed PB or UAV initial location ($R_{min} = 5 \times 10^4$ bit/s, $\varphi = -30$ dB).

4) *Total EE versus fixed PB or UAV initial location:* Fig. 10 shows the total EE versus the fixed PB location or the UAV initial location under two schemes, i.e., our proposed Algorithm 1 and the fixed PB based BackCom-HTT scheme. The total EE of both schemes increases with shorter distance from the UAV initial location or the PB location to the IoT nodes. It is easy to be verified that the harvested energy utilization and the throughput increases with short communication distance, which improves the EE. Specifically, the total EE of the fixed PB based BackCom-HTT scheme is very low when the distance from the PB to the IoT nodes is small, i.e., $(-12, 0)$, $(-11, 0)$ and $(-10, 0)$. This is because that the minimum throughput requirement of some users cannot be met, and none of the users could meet this requirement after the PB location is farther than $(-12, 0)$. Then the total EE significantly increases with shorter distance from the PB to the IoT nodes with less increasing rate. Also, the increasing trend of the total EE of our proposed algorithm is very stable, which is due to the high mobility of the UAV. Since the UAV works as a mobile power station, it can quickly fly to the region, where all the IoT nodes are located. Thus, the impact of the small distance difference of initial UAV locations on the EE is not obvious.

However, our proposed algorithm gain much more total EE than the fixed PB based BackCom-HTT scheme does. This is due to the high propagation loss of the long distance from the fixed PB to the IoT nodes, and the energy harvested by the IoT nodes is much decreased due to the same reason. Such high propagation loss seriously degrades the total EE performance as illustrated in Fig. 10. In addition, the EE gap between the two schemes becomes small, since the propagation loss difference between the fixed PB and the UAV is becoming small, which leads to this small EE gap.

E. Throughput Versus R_{min}

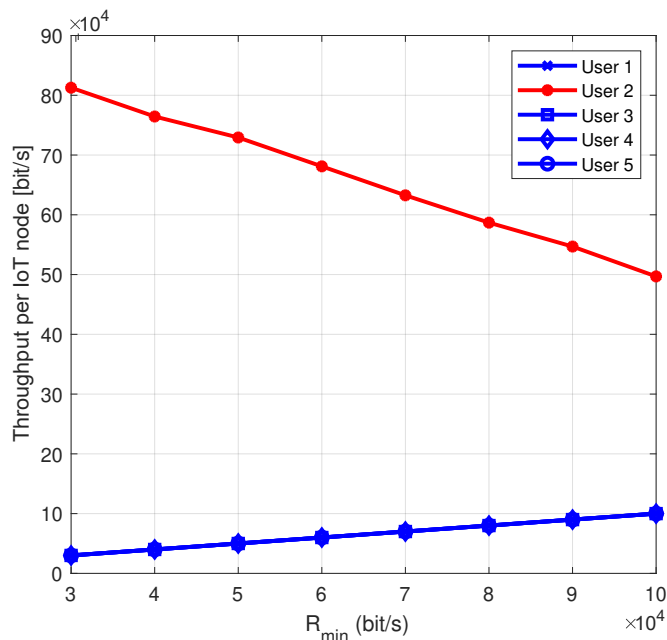


Fig. 11: Throughput versus minimum throughput requirement R_{min} ($\varphi = -30$ dB).

Fig. 11 illustrates the throughput of individual node versus R_{min} . It can be found that the throughput of IoT node 2, node 3, node 4, node 5 is identical to the corresponding R_{min} , i.e., 3, 4, 5, 6, 7, 8 and 9×10^4 bits/s, respectively. However, the throughput of IoT node 2 is much higher than R_{min} . This is because that we aim to maximize the total EE of all the IoT nodes, most time is allocated to IoT node 2 since it can provide more EE than other IoT nodes do due to better channel condition from itself to the UAV and to the reader. This allows IoT node 2 to gain much more throughput. Meanwhile, the minimum throughput requirement of other IoT nodes needs to be met, thus, other IoT node's throughput only needs to equal to R_{min} for achieving maximum EE of all the IoT nodes. In addition, the throughput of IoT node 2 gradually decreases with higher R_{min} . Since more time is allocated to other IoT nodes for meeting their minimum throughput requirement when increasing R_{min} , the throughput of IoT node 2 drops with less given transmit time.

VI. CONCLUSIONS

In this paper, we have investigated the total EE maximization of all the IoT nodes in a UAV-enabled hybrid BackCom-HTT network. Since the optimization problem is non-convex, we have proposed a Dinkelbach based iterative algorithm to first transform the problem into a more tractable subtractive form, then use a BCD method to decompose the transformed problem into two sub-problems, where the communication resource allocation subproblem is solved by employing the Lagrangian dual method and the UAV trajectory optimization subproblem is solved by applying the SCP technique. Simulation results demonstrate that the total EE performance of our proposed algorithm is much better than the benchmark schemes, i.e., the UAV-enabled backscatter scheme, the UAV-enabled HTT scheme, the energy consumption minimization scheme, and the fixed PB based hybrid BackCom-HTT scheme. Moreover, our results show the total EE of all the ground IoT nodes increases for a lower throughput requirement, higher backscatter performance gap and higher UAV maximum speed under all the considered schemes. In addition, our proposed algorithm allocates more time for BackCom and/or active transmission to the IoT nodes with better channel conditions for improving the total EE of all the IoT nodes, while guaranteeing the other IoT nodes meeting their minimum throughput requirement.

In our future work, we will extend this work to the case with multiple UAVs serving a large number of IoT nodes distributed over a large area, where the interference mitigation during BackCom and the trajectory optimization for multiple UAVs will be the main challenges to tackle. It will also be interesting to extend the proposed system model to the case of fixed wing UAVs or for online operation.

APPENDIX A

PROOF OF LEMMA 1

When P^u , \mathbf{Z} , $\boldsymbol{\tau}$, \mathbf{t} , \mathbf{P} and \mathbf{q} are given, the objective function in \mathbf{P}_1 monotonically increases with P^u since P^u only exists in the numerator of the objective function. Thus, the optimal UAV transmit power is obtained by its upper bound. Due to C4-C7 in \mathbf{P}_1 , they are used to obtain the lower bound of P^u , the upper bound of P^u is given by P_{max}^{uav} and we have $P^{u*} = P_{max}^{uav}$. The proof is completed.

APPENDIX B

PROOF OF LEMMA 2

Let us define two functions given by $f_1 = A \log_2 \left(1 + \frac{B}{C(H^2+F)} \right)$ and $f_2 = \frac{D}{H^2+F}$, where $A, B, C, D > 0$ are constants, f_1 and f_2 are both convex with respect to F . Since the first-order Taylor expansion of a convex function is a global under-estimator of the function values, for any $F_0 \geq 0$ we can obtain

$$f_1 \geq A \log_2 \left(1 + \frac{B}{C(H^2 + F_0)} \right) - \frac{A \log_2 e}{\left(1 + \frac{C(H^2 + F_0)}{B} \right)} (F - F_0), \quad (44)$$

$$f_2 \geq \frac{D}{H^2 + F_0} - \frac{D}{(H^2 + F_0)^2} (F - F_0). \quad (45)$$

By substituting $A = W\tau_{i,n}$, $B = \varphi P_{\max}^{uav} h_i^r X_{i,n} \beta_0 \mu$, $C = W\sigma^2 \tau_{i,n}$ and $D = P_{\max}^{uav} \eta \beta_0 \mu \left(\frac{\theta T}{N} - X_{i,n} \right)$ into (44) and (45), then (36) and (37) are obtained. Also, the equalities in (44) and (45) hold when $F = F_0$, thus, the equalities in (36) and (37) hold when $\mathbf{q}^0 = \mathbf{q}^l$. The proof is completed.

APPENDIX C

BENCHMARK SCHEMES

1) *UAV-enabled backscatter scheme*: In this scheme, we aim to maximize the EE of all the IoT nodes, where the overall time period T is allocated to the IoT nodes for wireless energy transfer and BackCom. Accordingly, the optimization problem of this scheme is formulated as

$$\begin{aligned} \mathbf{P}_5 : \quad & \max_{\{\mathbf{Z}_n, \boldsymbol{\tau}_n, \mathbf{q}\}} \frac{\sum_{i=1}^M \sum_{n=1}^N W \tau_{i,n} \log_2 \left(1 + \frac{\varphi P_{\max}^{uav} h_{i,n}^u Z_{i,n} h_i^r}{W \sigma^2} \right)}{PC^B \sum_{i=1}^M \sum_{n=1}^N \tau_{i,n}} \\ \text{s.t.} \quad & \text{C7, C8;} \\ & \text{C1}' : 0 \leq Z_{i,n} \leq 1, \tau_{i,n} \geq 0, \forall i, \forall n; \\ & \text{C2}' : \sum_{i=1}^M \tau_{i,n} = \frac{T}{N}, \forall n; \\ & \text{C3}' : \sum_{n=1}^N R_{i,n}^B \geq R_{min}, \forall i; \\ & \text{C4}' : EH_i - \sum_{n=1}^N PC^B \tau_{i,n} \geq 0, \forall i; \end{aligned} \quad (46)$$

2) *UAV-enabled HTT scheme*: In this scheme, we aim to maximize the EE of all the IoT nodes, where the IoT nodes only harvest energy from the UAV during the first time period and use the harvested energy to transmit

information during the second time period. Accordingly, the optimization problem of this scheme is formulated as

$$\begin{aligned}
\mathbf{P}_6 : \quad & \max_{\{\theta, \mathbf{t}, \mathbf{P}, \mathbf{q}\}} \frac{\sum_{i=1}^M W t_i \log_2 \left(1 + \frac{P_i h_i^r}{W \sigma^2} \right)}{\sum_{i=1}^M t_i (P_i + PC^H)} \\
\text{s.t.} \quad & \\
& \text{C7, C8;} \\
& \text{C1}'' : 0 \leq \theta \leq 1, 0 \leq P_i \leq P_{\max}^{node}, \forall i; \\
& \text{C2}'' : \sum_{i=1}^M \tau_{i,n} = \frac{\theta T}{N}, \sum_{i=1}^M t_i = (1 - \theta)T; , \forall n \\
& \text{C3}'' : \sum_{i=1}^M R_i^H \geq R_{\min}, \\
& \text{C4}'' : EH_i - \sum_{i=1}^M t_i (P_i + PC^H) \geq 0, \forall i.
\end{aligned} \tag{47}$$

3) *Energy consumption minimization scheme*: In this scheme, we aim to minimize the total energy consumption, where other constraints in \mathbf{P}_1 keep the same. Accordingly, the optimization problem of this scheme is formulated as

$$\begin{aligned}
\mathbf{P}_7 : \quad & \min_{\{\theta, \mathbf{Z}_n, \tau_n, \mathbf{t}, \mathbf{P}, \mathbf{q}\}} PC^B \sum_{i=1}^M \sum_{n=1}^N \tau_{i,n} + \sum_{i=1}^M t_i (P_i + PC^H) \\
\text{s.t.} \quad & \\
& \text{C1} - \text{C8}.
\end{aligned} \tag{48}$$

4) *Fixed PB based backscattering with HTT scheme*: In this scheme, we aim to maximize the EE of all the IoT nodes, where a fixed PB instead of the UAV is located outside the IoT node region. In particular, the first time period allocated to the BackCom is divided into M time slots with i th time slot allocated to i th IoT node by employing TDMA, which is the same as that in active transmission. Accordingly, the optimization problem of this scheme is formulated as

$$\begin{aligned}
\mathbf{P}_8 : \quad & \max_{\{\theta, \mathbf{Z}_n, \tau_n, \mathbf{t}, \mathbf{P}\}} \frac{\sum_{i=1}^M (R_i^B + R_i^H)}{EC_{sum}^{PB}} \\
\text{s.t.} \quad & \\
& \text{C1;} \\
& \text{C2}''' : 0 \leq P^B \leq P_{\max}^B, 0 \leq P_i \leq P_{\max}^{node}, \forall i; \\
& \text{C3}''' : \sum_{i=1}^M \tau_i = \theta T, \sum_{i=1}^M t_i = (1 - \theta)T; \\
& \text{C4}''' : R_i^B + R_i^H \geq R_{\min}, \forall i; \\
& \text{C5}''' : EH_i^{PB} - EC_{sum}^{PB} \geq 0, \forall i,
\end{aligned} \tag{49}$$

where $R_i^B = W \tau_i \log_2 \left(1 + \frac{\varphi P_{\max}^B h_i^B Z_i h_i^r}{W \sigma^2} \right)$, $EH_i^{PB} = \sum_{n=1}^N P^u \eta h_i^u (\theta T - \tau_i Z_i)$ and $EC_{sum}^{PB} = \sum_{i=1}^M (PC^B \tau_i + t_i (PC^H + P_i))$, P_{\max}^B and h_i^B denote the maximum PB transmit power and the channel power gain from the PB to the IoT

nodes, respectively. P_{max}^B is set the same as P_{max}^{uav} for comparison. Based on the algorithms proposed to solve \mathbf{P}_1 , we employ the same methods to solve \mathbf{P}_5 , \mathbf{P}_6 , \mathbf{P}_7 and \mathbf{P}_8 , respectively. The optimization process for these four schemes is omitted for saving space.

REFERENCES

- [1] Q. Wu, W. Chen, D. W. K. Ng, and R. Schober, "Spectral and energy-efficient wireless powered IoT networks: NOMA or TDMA?," *IEEE Transactions on Vehicular Technology*, vol. 67, no. 7, pp. 6663–6667, 2018.
- [2] S. Bi, Y. Zeng, and R. Zhang, "Wireless powered communication networks: an overview," *IEEE Wireless Communications*, vol. 23, no. 2, pp. 10–18, 2016.
- [3] S. Bi, C. K. Ho, and R. Zhang, "Wireless powered communication: opportunities and challenges," *IEEE Communications Magazine*, vol. 53, no. 4, pp. 117–125, 2015.
- [4] K. W. Choi, L. Ginting, A. A. Aziz, D. Setiawan, J. H. Park, S. I. Hwang, D. S. Kang, M. Y. Chung, and D. I. Kim, "Toward realization of long-range wireless-powered sensor networks," *IEEE Wireless Communications*, vol. 26, no. 4, pp. 184–192, 2019.
- [5] B. Lyu, C. You, Z. Yang, and G. Gui, "The optimal control policy for RF-powered backscatter communication networks," *IEEE Transactions on Vehicular Technology*, vol. 67, no. 3, pp. 2804–2808, 2018.
- [6] X. Kang, Y. Liang, and J. Yang, "Riding on the primary: A new spectrum sharing paradigm for wireless-powered IoT devices," *IEEE Transactions on Wireless Communications*, vol. 17, no. 9, pp. 6335–6347, 2018.
- [7] H. Yang, Y. Ye, and X. Chu, "Max-min energy-efficient resource allocation for wireless powered backscatter networks," *IEEE Wireless Communications Letters*, pp. 1–1, 2020.
- [8] Y. Ye, L. Shi, X. Chu, and G. Lu, "Throughput fairness guarantee in wireless powered backscatter communications with htt," *IEEE Wireless Communications Letters*, pp. 1–1, 2020.
- [9] S. H. Kim and D. I. Kim, "Hybrid backscatter communication for wireless-powered heterogeneous networks," *IEEE Transactions on Wireless Communications*, vol. 16, no. 10, pp. 6557–6570, 2017.
- [10] B. Lyu, H. Guo, Z. Yang, and G. Gui, "Throughput maximization for hybrid backscatter assisted cognitive wireless powered radio networks," *IEEE Internet of Things Journal*, vol. 5, no. 3, pp. 2015–2024, 2018.
- [11] D. T. Hoang, D. Niyato, P. Wang, and D. I. Kim, "Optimal time sharing in RF-powered backscatter cognitive radio networks," in *2017 IEEE International Conference on Communications (ICC)*, pp. 1–6, 2017.
- [12] L. Shi, R. Q. Hu, J. Gunther, Y. Ye, and H. Zhang, "Energy efficiency for rf-powered backscatter networks using htt protocol," *IEEE Transactions on Vehicular Technology*, vol. 69, no. 11, pp. 13932–13936, 2020.
- [13] H. Ju and R. Zhang, "Throughput maximization in wireless powered communication networks," *IEEE Transactions on Wireless Communications*, vol. 13, no. 1, pp. 418–428, 2014.
- [14] J. Xu, Y. Zeng, and R. Zhang, "UAV-enabled wireless power transfer: Trajectory design and energy optimization," *IEEE Transactions on Wireless Communications*, vol. 17, no. 8, pp. 5092–5106, 2018.
- [15] L. Xie, J. Xu, and R. Zhang, "Throughput maximization for UAV-enabled wireless powered communication networks," *IEEE Internet of Things Journal*, vol. 6, no. 2, pp. 1690–1703, 2019.
- [16] M. Hua, L. Yang, C. Li, Q. Wu, and A. L. Swindlehurst, "Throughput maximization for UAV-aided backscatter communication networks," *IEEE Transactions on Communications*, vol. 68, no. 2, pp. 1254–1270, 2020.
- [17] L. Xie, J. Xu, and Y. Zeng, "Common throughput maximization for uav-enabled interference channel with wireless powered communications," *IEEE Transactions on Communications*, vol. 68, no. 5, pp. 3197–3212, 2020.
- [18] C. Zhan, Y. Zeng, and R. Zhang, "Energy-efficient data collection in UAV enabled wireless sensor network," *IEEE Wireless Communications Letters*, vol. 7, no. 3, pp. 328–331, 2018.
- [19] C. You and R. Zhang, "3d trajectory optimization in rician fading for uav-enabled data harvesting," *IEEE Transactions on Wireless Communications*, vol. 18, no. 6, pp. 3192–3207, 2019.

- [20] J. Lyu, Y. Zeng, and R. Zhang, "Uav-aided offloading for cellular hotspot," *IEEE Transactions on Wireless Communications*, pp. 1–1, 2018.
- [21] Y. Zeng, R. Zhang, and T. J. Lim, "Throughput maximization for UAV-enabled mobile relaying systems," *IEEE Transactions on Communications*, vol. 64, no. 12, pp. 4983–4996, 2016.
- [22] M. Hua, Y. Wang, M. Lin, C. Li, Y. Huang, and L. Yang, "Joint CoMP transmission for UAV-aided cognitive satellite terrestrial networks," *IEEE Access*, vol. 7, pp. 14959–14968, 2019.
- [23] Q. Wu, Y. Zeng, and R. Zhang, "Joint trajectory and communication design for multi-UAV enabled wireless networks," *IEEE Transactions on Wireless Communications*, vol. 17, no. 3, pp. 2109–2121, 2018.
- [24] Y. Liang, R. Long, Q. Zhang, J. Chen, H. V. Cheng, and H. Guo, "Large intelligent surface/antennas (lisa): Making reflective radios smart," *Journal of Communications and Information Networks*, vol. 4, no. 2, pp. 40–50, 2019.
- [25] N. Van Huynh, D. T. Hoang, X. Lu, D. Niyato, P. Wang, and D. I. Kim, "Ambient backscatter communications: A contemporary survey," *IEEE Communications Surveys & Tutorials*, vol. 20, no. 4, pp. 2889–2922, 2018.
- [26] B. Smida and S. Khaledian, "ReflectFX: In-band full-duplex wireless communication by means of reflected power," *IEEE Transactions on Communications*, vol. 65, no. 5, pp. 2207–2219, 2017.
- [27] M. Ismail, W. Zhuang, E. Serpedin, and K. Qaraqe, "A survey on green mobile networking: From the perspectives of network operators and mobile users," *IEEE Communications Surveys & Tutorials*, vol. 17, no. 3, pp. 1535–1556, 2015.
- [28] W. Dinkelbach, "On nonlinear fractional programming," *Management Science*, vol. 13, pp. 492–498, March 1967, Available: <http://www.jstor.org/stable/2627691>.
- [29] S. Boyd, *Convex optimization*. Cambridge, UK: Cambridge University Press, 2004.
- [30] G. Yang, R. Dai, and Y. C. Liang, "Energy-efficient uav backscatter communication with joint trajectory design and resource optimization," *IEEE Transactions on Wireless Communications*, vol. 20, no. 2, pp. 926–941, 2021.
- [31] H. Zhang, C. Jiang, N. C. Beaulieu, X. Chu, X. Wen, and M. Tao, "Resource allocation in spectrum-sharing OFDMA femtocells with heterogeneous services," *IEEE Transactions on Communications*, vol. 62, no. 7, pp. 2366–2377, 2014.
- [32] J. Gondzio and T. Terlaky, "A computational view of interior point methods," *JE Beasley. Advances in Linear and Integer Programming. Oxford Lecture Series in Mathematics and its Applications*, vol. 4, pp. 103–144, 1996.
- [33] F. Zhou, Y. Wu, R. Q. Hu, and Y. Qian, "Computation rate maximization in uav-enabled wireless-powered mobile-edge computing systems," *IEEE Journal on Selected Areas in Communications*, vol. 36, no. 9, pp. 1927–1941, 2018.
- [34] Q. Wu, W. Chen, D. W. Kwan Ng, J. Li, and R. Schober, "User-centric energy efficiency maximization for wireless powered communications," *IEEE Transactions on Wireless Communications*, vol. 15, no. 10, pp. 6898–6912, 2016.